PCCP

Accepted Manuscript

ROYAL SOCIETY OF CHEMISTRY

www.rsc.org/pccp

PCCP

RSCPublishing

REVIEW ARTICLE

Mid-infrared optical parametric oscillators and frequency combs for molecular spectroscopy

Cite this: DOI: 10.1039/x0xx00000x

M. Vainio,[a,b] and L. Halonen[a]

Received 00th January 2012,
Accepted 00th January 2012

DOI: 10.1039/x0xx00000x

www.rsc.org/

Nonlinear optical frequency conversion is one of the most versatile methods to generate wavelength-tunable laser light in the mid-infrared region. This spectral region is particularly important for trace gas detection and other applications of molecular spectroscopy, because it accommodates the fundamental vibrational bands of several interesting molecules. In this article, we review the progress of the most significant nonlinear optics instruments for widely tunable, high-resolution mid-infrared spectroscopy: continuous-wave optical parametric oscillators and difference frequency generators. We extend our discussion to mid-infrared optical frequency combs, which are becoming increasingly important spectroscopic tools, owing to their capability for highly sensitive and selective parallel detection of several molecular species. To illustrate the potential and limitations of mid-infrared sources based on nonlinear optics, we also review typical uses of these instruments in both applied and fundamental spectroscopy.

1 Introduction

Besides fundamental research of physical chemistry, molecular absorption spectroscopy has a number of applications in detection and quantification of small traces of biomarkers, toxics, or other interesting molecules in gaseous samples. Examples of these application are atmospheric and environmental monitoring [1], as well as real-time medical diagnostics by analysis of exhaled breath [2]. Some of the key parameters of trace gas detection and molecular fingerprinting are sensitivity, speed, selectivity, and the capability of detecting multiple species simultaneously.

From the technology point of view, the highest sensitivity, i.e., the capability of detecting small concentrations can usually be obtained by using laser spectroscopy. This results from the high brightness and spatial coherence of lasers, which makes it possible to reach high signal-to-noise ratios and long absorption path lengths. The sensitivity can be further increased by using multipass cells and enhancement cavities. The high brightness also means that the high measurement sensitivity can be obtained with a short averaging time, which leads to fast, in practice real-time measurements. Also the spectroscopic selectivity, i.e., the capability of resolving one molecular absorption line or species from another, is superior in laser spectroscopy, as compared to more conventional methods. In particular, the high spectral resolution and hence high selectivity can be obtained by using single-mode continuous-wave lasers – a typical single-mode continuous-wave (CW) laser used for spectroscopy has a linewidth of the order of 10 MHz (~3×10^{-4} cm^{-1}) or less, well sufficient to resolve Doppler-broadened mid-infrared absorption lines that have linewidths of the order of 100 MHz. For comparison, only the largest Fourier transform infrared (FTIR) interferometers are capable of yielding even comparable spectral resolution with conventional incoherent light sources [3]. While the single-frequency CW lasers are ideal for high-resolution spectroscopy, they cannot be used to detect several molecular species simultaneously. The optical frequency comb, which is a light source that combines all the preferable characteristics of CW lasers with a broad spectral bandwidth, has recently provided an elegant solution to this problem [4,5,6,7].

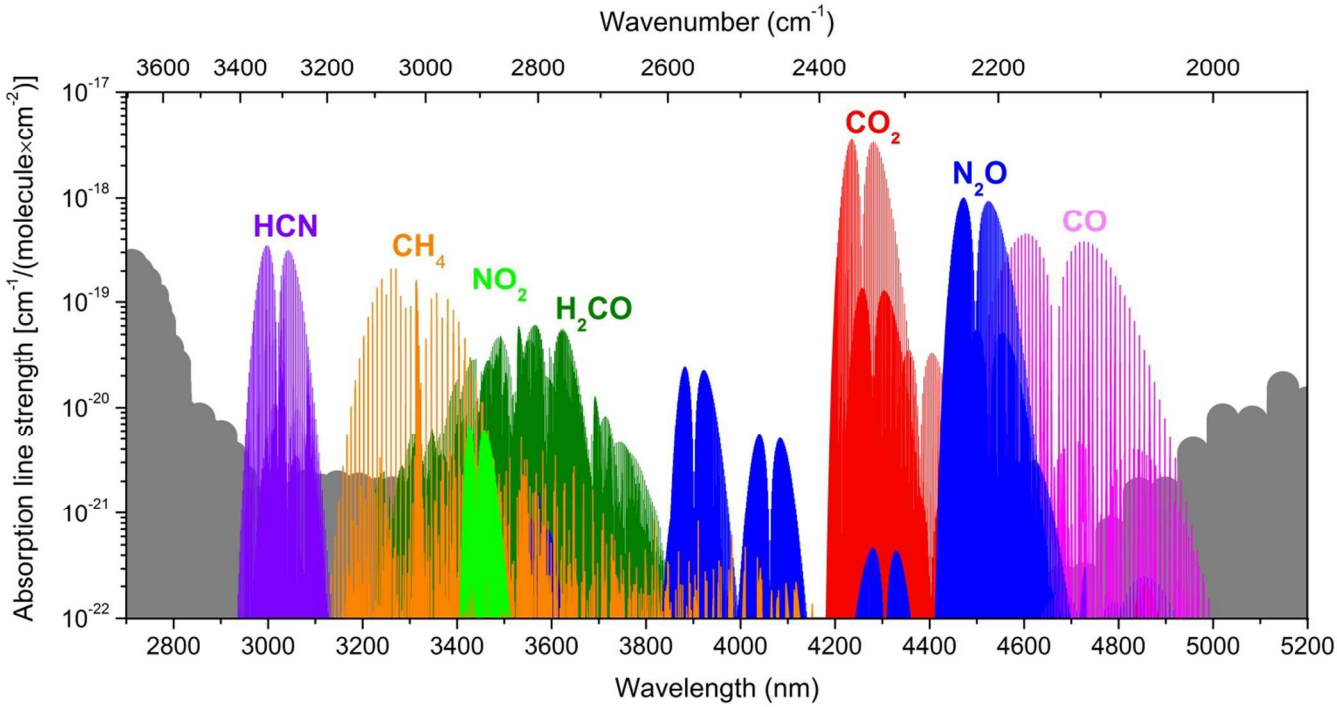

Figure 1. Absorption spectra of some important trace gases in the wavelength region between 3 and 5 µm. The solid grey background shows the water vapour absorption, which quickly increases outside of the atmospheric window. Note that the figure only shows the absorption line strengths per molecule, *not* taking into account the abundances of the molecular species. The molecular line data are from the HITRAN 2012 database.

From the fundamental point of view, the detection sensitivity can be optimised by doing spectroscopy in the mid-infrared region, where many trace gas molecules have their strongest absorption features. The definition of mid-infrared is somewhat ambiguous and depends on the application. Here, we define the mid-infrared region as 2.5-25 µm (or, 400-4000 cm^{-1}, or 12-120 THz). Most trace gas molecules have their fundamental rotational-vibrational bands in this region. These fundamental rovibrational bands are typically at least two orders of magnitude stronger than the respective overtone bands. So-called atmospheric window at 3-5 µm (2000-3300 cm^{-1}) is particularly important, as it occupies the strongest absorption bands of the carbohydrates (CH stretch) and molecules with NH or OH stretching vibration. It is also worth noting that within the atmospheric window water vapour absorption is relatively small. This is useful in certain applications, such as atmospheric and environmental monitoring, where the measurement of trace gas spectra is often complicated by strong spectral features of the abundant water molecule. Figure 1 shows the absorption spectra of some of the most important trace gas molecules in the spectral region between 3 and 5 µm.

Mid-infrared molecular spectroscopy, in particular its application to trace gas analysis, has progressed significantly during the past two decades, owing to the development of coherent mid-infrared sources, detectors, and methods. One of the important enabling technological advances has been the invention of room-temperature quantum cascade lasers and interband cascade lasers, which have extended the operating range of tunable semiconductor lasers from the visible and near-infrared to the mid-infrared. The present status of mid-infrared quantum cascade laser is reviewed, e.g., in [8]. An equally important step has been the development of quasi-phase-matched (QPM) nonlinear crystals [9], a technology that makes it possible to transfer the favorable characteristics of near-infrared solid-state lasers with high efficiency to practically any wavelength in the mid-infrared region. One of the many benefits of the QPM frequency converters is the broad wavelength tuning range, which makes them ideal for multispecies trace gas detection. The most important material for QPM nonlinear mid-infrared frequency conversion is periodically poled lithium niobate (PPLN). The transmission range of PPLN extends up to ~5 µm [10], which makes it suitable for accessing one of the important atmospheric windows (Fig. 1).

The purpose of this article is to review the current state and recent developments of coherent mid-infrared sources based on optical parametric processes, i.e., on nonlinear optical frequency conversion. Good practical introductions to fundamentals of various nonlinear optical phenomena can be found, for example, in references [11,12]. Here, we focus on methods that can be used for high-resolution molecular spectroscopy, since high spectral resolution is typically required to acquire detailed information about molecular structure and to perform selective multispecies trace gas analysis. This sets our focus to continuous-wave optical parametric oscillators (OPOs); the linewidth of pulsed (nanosecond and picosecond) sources is typically too large for high-resolution applications.

For the sake of completeness, we also discuss CW difference frequency generation (DFG), a simple method which shares many favorable properties of OPOs. While the mid-infrared DFG sources can nowadays in many applications be replaced by quantum cascade lasers and interband cascade lasers, they can still offer certain benefits especially in laboratory experiments. Also, understanding of the basics of DFG helps to grasp the essentials of OPOs that still provide a unique combination of high output power and broad wavelength tunability in the mid-infrared region.

We extend our review to mid-infrared frequency combs, which can be generated by nonlinear frequency conversion methods, such as DFG and synchronously pumped OPOs. These frequency combs are becoming increasingly important for multispecies molecular fingerprinting, owing to the large instantaneous mid-infrared bandwidth that can exceed a full octave. Although a laser frequency comb is in general based on a pulsed femtosecond source, it produces a spectrum that consists of discrete peaks. This makes OFCs suitable for high-resolution spectroscopic studies. In fact, in the frequency domain, an OFC can be considered as a source that emits up to a million CW laser frequencies simultaneously.

This paper is organized as follows: In Section 2, we review the basics, instrumentation, as well as the recent developments of CW difference-frequency generators, OPOs, and parametric OFCs. The latter half of the paper, Section 3, is dedicated to the use of these instruments both in trace gas analysis and fundamental research. In order to give a comprehensive overview of the possibilities and limitations of mid-infrared parametric sources in high-resolution molecular spectroscopy, we have selected examples that cover a wide variety of different applications. We also briefly review some of the most typical spectroscopic methods used in these applications.

2 Mid-infrared generation by parametric processes

2.1 Difference frequency generation

Basics

In difference frequency generation, two laser beams are overlapped and focused into a nonlinear optical crystal (Fig. 2). These beams are referred to as pump (p) and signal (s) beams. The beam at the shorter wavelength is named, by convention, the pump beam. If the pump-beam power is sufficiently high, its energy is efficiently transferred to the signal beam while propagating in the crystal. As a result, a third beam, so-called idler (i) beam, is produced. The frequency ν_i of the idler beam is given as a function of pump and signal frequencies, ν_p and ν_s, respectively, by the law of energy conservation:

$$h\nu_i = h\nu_p - h\nu_s\,, \qquad (1)$$

where h is Planck's constant. The vacuum wavelengths of the beams are $\lambda_x = c/\nu_x$, where c is the speed of light in vacuum. A typical example of mid-infrared generation by a DFG process is the mixing of light from a high-power Nd:YAG laser (λ_p = 1064 nm) with light of a tunable diode laser (λ_s ~ 1550 nm), producing an idler beam at λ_i ~ 3400 nm.

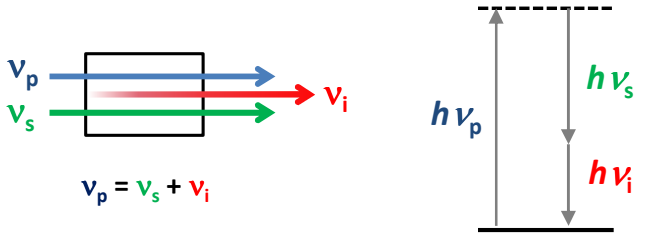

Figure 2. The principle of DFG. Left: The pump and signal beams are focused into a nonlinear crystal, producing an output beam (idler), which fulfils Eq. (1). Note that the beams need to overlap in the crystal in order to ensure efficient flow of energy the idler beam. Right: the process can be illustrated by an energy level diagram, where the dashed line indicates a virtual state.

In order DFG to be efficient, the process also has to conserve momentum – this condition is often referred to as phase-matching condition, which is

$$\Delta k = 0. \qquad (2)$$

For a process where all interacting beams propagate collinearly the wavevector mismatch Δk is, in a general, defined as

$$\Delta k = k_p - k_s - k_i, \qquad (3)$$

where $k_x = 2\pi n_x/\lambda_x$ is the angular wavenumber, with n_x being the refractive index of the material at the respective wavelength λ_x.

At $\Delta k \sim 0$, the idler waves generated at different parts of the crystal sum up coherently, so that the idler power increases monotonically while propagating in the crystal. The phase-matched idler power $P_{i,0} = P_i(\Delta k = 0)$ is proportional to the product of the pump power (P_p) and signal power (P_s), and can be calculated from [13,14,15,16]

$$P_{i,0} = \frac{32\pi d_{eff}^2 L}{\varepsilon_0 c \lambda_i^2 n_i(\lambda_p n_s + \lambda_s n_p)} P_p P_s h(\mu, \xi_p, \xi_s)\,, \qquad (4)$$

where d_{eff} is the effective second order nonlinear coefficient of the crystal, ε_0 is the vacuum permittivity, and L is the length of the crystal. Function $h(\mu, \xi_p, \xi_s)$ depends on the ratio of the input wavenumbers $\mu = k_s/k_p$, as well on the tightness of focusing of the beams, $\xi_x = L\lambda_x/2\pi w_x^2 n_x$, where w_x is the $1/e^2$-intensity radius of the beam waist. As a general rule of thumb, this function reaches the maximum value when the beams overlap and $\xi_p \sim \xi_s \sim 1$, which corresponds to confocal focusing [11,13,14,17]. Here, it is assumed that the interacting beams have Gaussian intensity profiles, which is typical for lasers. As an example, let us consider DFG between a λ_p = 1064 nm Nd:YAG-laser and a λ_s = 1550 nm diode laser in a 50-mm long PPLN crystal. Both input beams, pump and signal, are linearly polarized with extraordinary (e) polarization, which in the case

of PPLN maximizes the effective nonlinear coefficient $d_{\text{eff}} \sim 14$ pm/V*. The refractive indexes are $n_p \sim n_s \sim n_i \sim 2$ [10]. Confocal focusing, $w_p = 65$ μm and $w_s = 95$ μm ($\xi_p = \xi_s = 1$), is assumed, which leads to $h(\mu, \xi_p, \xi_s) \sim 0.3$ [14]. With $P_p = 0.5$ W and $P_s = 20$ mW, we obtain $P_i^0 = 30$ μW at 3.4 μm.

Difference frequency generation is a parametric process, which means that there is no transfer of energy between the optical field and the nonlinear crystal. Unlike a laser gain material, the crystal does not store energy, which makes the parametric processes fast – the response time of the electric polarisation to an optical field is of the order of 10^{-15} s. Also, as the process does not rely on transitions between the energy levels of the crystal material, efficient frequency conversion is possible within the entire transmission spectrum of the material, as long as the energy-conservation and phase-matching conditions (Eqs. 1 and 2) can be met.

Phase matching

One possible method to achieve $\Delta k \sim 0$ is birefringent phase matching, which relies on the anisotropy of certain nonlinear crystals [11,12,16]. The refractive index depends on the wavelength (dispersion), but also on the light polarization and propagation direction relative to the crystal lattice. By choosing the light propagation directions and polarizations in the crystal properly, it is, in some cases, possible to obtain a situation where the phase-matching condition is fulfilled. This method, however, has limitations. First of all, the polarizations that provide phase matching do not usually produce the highest possible nonlinearity – the nonlinear coefficient is, in general, a function of polarization and propagation direction. Secondly, as the polarizations of the beams are different, their propagation directions in the crystal often differ due to the Poynting-vector walk-off, which leads to spatial separation of the beams, hence limiting the interaction length and conversion efficiency.

The reduction of DFG conversion efficiency due to the aforementioned reasons can be avoided by using quasi phase matching [9,11,16]. In QPM, the crystal polarity is inverted every wave-mixing coherence-length $l_{\text{coh}} = \pi/|\Delta k|$, i.e., at the point where the generated field would otherwise come out of phase compared to the previously generated field. This ensures monotonic increase of the generated mid-infrared power, as is illustrated in Fig. 3. The QPM period is usually denoted by symbol Λ, and the phase-mismatch becomes

$$\Delta k_{QPM} = \Delta k - \frac{2\pi}{\Lambda} = k_p - k_s - k_i - \frac{2\pi}{\Lambda}, \qquad (5)$$

where $\Delta k_{QPM} = 0$ is trivially achieved if $\Lambda = 2l_{\text{coh}}$. Note that we use the term phase-matched for both birefringent phase matching and quasi phase matching. Therefore, from now on, we don't explicitly refer to QPM with symbol Δk_{QPM}. Instead, we shall use the notation $\Delta k = 0$ to describe phase matching in general, no matter how it's in practice achieved.

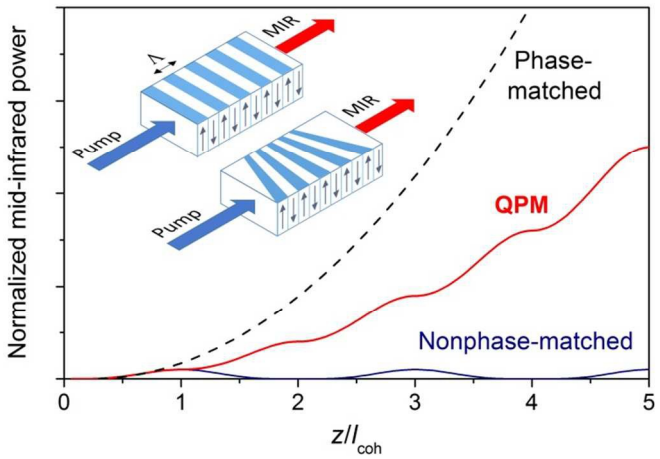

Figure 3. Parametrically generated mid-infrared power as a function of propagation distance z in the nonlinear crystal. In a nonphase-matched case the energy oscillates between the fundamental and parametrically generated fields with a period of $2l_{\text{coh}}$. Monotonic growth of the parametrically generated power is ensured by QPM, where the crystal polarity is inverted every l_{coh}. The inset schematically shows examples of two different QPM crystals for mid-infrared (MIR) generation: one with a uniform Λ and another with a fan-out structure.

The QPM technique has several advantages over birefringent phase matching: (1) the polarizations of the light beams can be freely chosen so as to access the direction of highest nonlinearity, (2) one can achieve so-called noncritical phase matching, which means that all three waves (p, s, i) propagate collinearly without spatial walk-off, (3) quasi phase matching can also be used for non-birefringent materials, such as GaAs, (4) it is possible to tailor phase matching for practically any wavelength within the transparency range of the crystal material by proper design of Λ.

Crystal materials

A typical nonlinear material for parametric generation of coherent mid-infrared light is periodically-poled lithium niobate ($LiNbO_3$), PPLN, which is transparent between 0.4 and 5 μm [10,18]. Quasi phase matching in this case is achieved by periodical poling of the crystal. This can be done by applying an intense electric field between the crystal surfaces, using electrodes that are patterned with the desired QPM structure [9]. If the electric field is stronger than the internal (coercive) field of the crystal (> 21 kV/mm for undoped congruent $LiNbO_3$ [9]), the crystal structure is permanently inverted. The same method can also be used for other ferroelectric crystals. The most common of these, after PPLN, are periodically-poled lithium tantalite $LiTaO_3$ (PPLT, transparent *ca.* 0.3 – 5.5 μm [19]) and periodically-poled potassium titanyl phoshate (PPKTP, transparent *ca.* 0.4 – 3.2 μm [20]). The $LiNbO_3$ and $LiTaO_3$ crystals are commonly doped with metal ions to reduce photorefractive damage, which can lead to severe complications, including beam distortion and even permanent damage of the crystal [21]. As an example, magnesium oxide

* Note that, in the case of quasi phase matching, such as PPLN, $d_{\text{eff}} = (2/\pi)d_{\text{eff},0}$, where $d_{\text{eff},0}$ is the effective nonlinear coefficient of the bulk material [9]. Also, the nonlinear coefficient is wavelength dependent, which can be taken into account using Miller's delta, which is an empirical formula [9]).

doped PPLN, MgO:PPLN, is the most commonly used material in CW mid-infrared DFG. Photorefractive damage is a problem especially with short (< 1 μm) pump wavelengths and high pump intensities. Lithium tantalite is known to be more resistive to photorefractive damage than lithium niobate, and is often better suited for applications where a short pump wavelength, such as 532 nm, is used [22,23,24,25]. On the other hand, the nonlinearity of PPLT is smaller than that of PPLN [10].

While the ferroelectric crystals are transparent only up to ~ 4…5 μm wavelengths, other crystal materials can be used for mid-infrared generation at longer wavelengths. Birefringent phase matching can be obtained, e.g., with $AgGaS_2$, which is transparent between 0.47 and 13 μm [10]. Quasi phase matching has been demonstrated with GaAs, which is transparent between 0.9 and 17 μm and has an extremely large nonlinear coefficient: $d_{\mathrm{eff}}(\mathrm{GaAs}) \sim 5\times d_{\mathrm{eff}}(\mathrm{LiNbO_3})$ [26]. Comparisons of some of the most commonly used mid-infrared nonlinear crystals are presented, for example, in Refs. [16,27,28]. Detailed information of the properties of these and many other nonlinear crystals can be found in D. N. Nikogosyan's book *Nonlinear Optical Crystals: A Complete Survey* [10], as well as in the SNLO database [29].

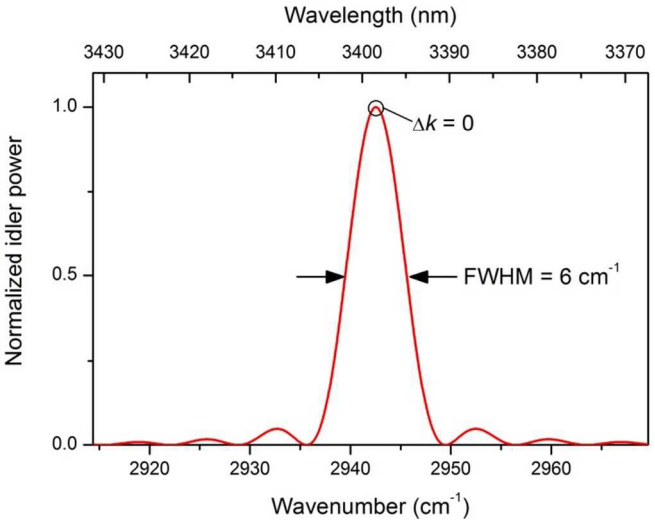

Figure 4. Calculated idler power vs. idler wavelength for a DFG process, where λ_p = 1064 nm pump laser beam is mixed with a tuneable signal laser beam (λ_s ~ 1.55 μm). The full width at half maximum (FWHM) of the phase-matching curve is 6 cm^{-1} (180 GHz), which is obtained with a 5-cm long PPLN crystal. Tuning of the idler wavelength across the phase-matching curve can be done by tuning the signal laser wavelength. The PPLN temperature and poling period used in the calculation are 325 K and 30.5 μm, respectively.

Wavelength tuning

As is indicated by Eq. 3, the phase-mismatch Δk depends on refractive indexes n_p, n_s, and n_i. These refractive indexes can be calculated using a Sellmeier equation, which is an empirical formula typically of the form [30]

$$n = a_1 + b_1 f_T + \frac{a_2 + b_2 f_T}{\lambda^2 - (a_3 + b_3 f_T)^2} + \frac{a_4 + b_4 f_T}{\lambda^2 - {a_5}^2} - a_6 \lambda^2, \quad (6)$$

where the Sellmeier coefficients, $a_1 \ldots a_6$, and $b_1 \ldots b_4$, can be experimentally determined. For example, the Sellmeier coefficients of PPLN have been reported by, e.g., Jundt [30] and Gayer *et al*. [31]. The temperature dependent parameter f_T can be taken into account using the definition given in [30] together with the data of Paul *et al*. [32]. The power of the idler beam as a function of phase-mismatch Δk approximately follows a $sinc^2$-curve [11,12]:

$$P_i = P_{i,0}\mathrm{sinc}^2(\Delta kL/2\pi)\,, \quad (7)$$

where $P_{i,0}$ is the phase-matched (Δk = 0) output power of the idler beam as calculated from Eq. 4. This formula, together with Eq. 3 (or Eq. 5 for QPM) and the refractive index data calculated from Eq. 6, can be used to estimate the DFG gain bandwidth and profile. An example of a typical DFG gain profile is shown in Fig. 4. Note that the gain bandwidth is inversely proportional to the crystal length. A large gain bandwidth can thus be obtained by using a short crystal, albeit at the cost of reduced conversion efficiency. The gain bandwidth and profile can also be tailored using different QPM structures, such as chirped or apodized poling [33,34].

According to Eq. (1), any change of the pump or signal frequency is converted to an idler frequency change of equal magnitude. This relation can be utilized for fast scanning of the idler frequency within the QPM gain bandwidth. For example, fast scanning of the 1550 nm DFB diode laser in the case of Fig. 4 can be used to tune the idler frequency over more than 180 GHz (6 cm^{-1}), which is sufficient to scan over several absorption lines of, e.g., nitrogen dioxide in this region. Larger changes of the idler wavelength require tuning of the phase matching. This can be done by varying the temperature and/or angle of the crystal. With quasi phase matching, coarse tuning is typically carried out by changing the QPM period. In practice, this can be done by mechanical translation of the crystal, which contains several parallel QPM periods or a "fan-out" structure (see the inset of Fig. 3). Typical phase-matching curves for 3 μm DFG by mixing of 1064 nm pump laser light and a wavelength-tuneable 1.5 μm laser are shown in Fig. 5.

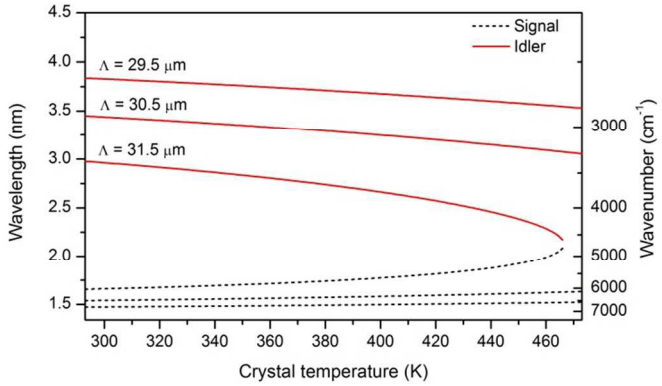

Figure 5. Calculated tuning of the phase-matched signal and idler wavelength pairs by tuning temperature of the PPLN crystal. The pump wavelength is fixed to λ_p = 1064 nm. The tuning curves are shown for three different QPM periods Λ.

SNLO software, which can be downloaded for free [29], is a handy tool to compute phase-matching wavelengths and tuning curves similar to those shown in Fig. 5. The program can be used to calculate both birefringent and quasi phase matching for the most commonly used nonlinear crystals. Several other parameters, such as the parametric gain bandwidths can also be estimated using SNLO.

Typical implementations

Mid-infrared generation by DFG can be realised using the scheme outlined in Fig. 2. The two input beams, pump and signal, are overlapped using a dichroic mirror and focused in the nonlinear crystal such that the confocal focusing condition is met, so as to maximize the *h*-term of Eq. (4) [13,14]. In addition, the light polarizations need to be adjusted in order maximize the nonlinear conversion efficiency and in some cases to obtain phase matching (birefringent phase matching). For instance, in the already discussed example of mixing 1064 nm and 1550 nm laser light, the most common solution is based on the use of a PPLN crystal, in which case both laser beams need to be linearly polarized with e-polarization. More details of this type of single-pass DFG in a bulk crystal can be found, e.g., in references [15,16,35].

The output power of the mid-infrared (idler) beam is proportional to the product of the incident pump and signal powers, see Eq. (4). Single-pass DFG using near-infrared diode lasers and a bulk PPLN crystal typically produces a few tens of microwatts in the mid-infrared region, as was shown in a previous example. This is not sufficient for certain applications, such as saturated absorption spectroscopy or photoacoustic spectroscopy. Moreover, an output power of at least several milliwatts is often needed for convenient use of mid-infrared wavelength meters and other measurement instruments.

The development of high-power fibre-optic amplifiers during the past two decades has provided a simple solution for power enhancement in mid-infrared DFG. In particular, polarization maintaining Yb-fibre amplifiers at ~1064 nm and Er-fibre amplifiers at ~1550 nm are readily available [35]. The optical gain bandwidths of these amplifiers support mid-infrared DFG over a large spectral range. As an example, more than 1 mW of coherent CW mid-infrared light tunable from 2.9 to 3.5 μm has been generated by mixing 550 mW of light from an Yb-fibre amplifier with 3.9 W of Er-fibre amplified light in a 5-cm long PPLN crystal [15]. Similar performance can also be achieved with high-power solid-state lasers [36]. For instance, over 2 mW of mid-infrared power tunable between 2.66 and 4.77 μm has been produced by mixing 1 W and 6 W of light from a Ti:sapphire laser and a Nd:YAG laser, respectively [37].

Another approach to improve the DFG output power is to increase the input power product either by placing the nonlinear crystal inside of the pump or signal laser (laser-intracavity DFG) or inside an external power build-up cavity (optical resonator). To avoid excessive experimental complexity, the build-up cavity is in practice designed for just one of the incident beams, while the other one passes the nonlinear crystal only once. Note that continuous build-up of the power in an external cavity requires the laser frequency to be locked to a cavity resonance, or vice versa, which increases the system complexity. Locking and other practical aspects of build-up cavities are discussed, e.g., in Refs. [38,39]. The power build-up factor of an external cavity is typically of the order of 10, which is sufficient to reach a mid-infrared output power of about 10 mW when combined with optical amplifiers [39]. For comparison, up to 30 mW of coherent, tunable continuous-wave light at 4.5 μm has been produced by performing DFG inside an injection-locked Ti:sapphire ring laser (~ 860 nm), while using a high-power (10 W) laser at 1064 nm as a signal source [40]. In a more recent work, several milliwatts of output power with a tuning range of more than 100 nm at ~5.4 μm was generated by intracavity DFG in an $AgGaS_2$ crystal, which was placed inside a dual-wavelength vertical external cavity surface emitting laser [41]. Despite the apparent multimode operation of the laser in the first demonstration, this compact scheme has potential in the field applications of trace gas spectroscopy.

Enhancement of the mid-infrared output power in DFG by use of optical amplifiers, build-up cavities, or laser intracavity DFG typically increases the system cost and complexity, which is disadvantageous in field applications of molecular spectroscopy. Difference-frequency generation in a quasi-phase-matched waveguide nonlinear crystal, on the other hand, is an elegant solution to increase the output power without adding much to system cost, size, or complexity [34,42,43,44,45]. A waveguide fabricated in the crystal concentrates the input laser fields in a small mode area of approximately 100 μm^2. As a result, the DFG conversion efficiency is improved by orders of magnitude as compared to DFG in a bulk crystal, where the intensity rapidly decreases due to divergence as the beams propagate in the crystal. As an example, more than 60 mW of CW mid-infrared power at 3.4 μm has been obtained by single-pass DFG in a 38-mm long Zn-doped PPLN waveguide using signal and pump powers of 558 mW and 444 mW, respectively [45]. Use of a chirped or apodized QPM instead of a uniform QPM structure reduces the output power by an order of magnitude, but provides a wavelength tuning range of tens of nanometres with a single waveguide, without the need to change the crystal temperature [34]. The input beams can be coupled into the waveguide in free space, by tightly focusing the beams into the input aperture of the waveguide [44]. However, owing to the small size of the aperture, fibre coupling is often a more convenient and reliable solution, especially in field applications [34]. Fibre-coupled waveguide crystals, as well as complete CW mid-infrared generators based on DFG are commercially available.

The precision of mid-infrared frequency scanning is, in addition to output power, a critical parameter of a DFG source used for high-resolution spectroscopy. Standard diode lasers and fibre laser, not to mention CW solid-state lasers, possess sufficiently small linewidth (< 30 MHz, or 0.001 cm^{-1}) and high frequency stability (< 300 MHz/min, or 0.01 cm^{-1}/min) for applications like trace gas detection. Certain applications in frequency metrology or fundamental research of molecules, for instance, require much better precision. Especially the long-

term stability of the mid-infrared frequency can be improved by several orders of magnitude by locking the near-infrared pump and signal laser frequencies to a stabilized optical frequency comb. Moreover, this approach makes it possible to control the mid-infrared frequency scans with an extremely high resolution and accuracy, even down to the kHz-level [46]. Optical frequency comb referenced DFG sources are discussed in more detail in Section 3.

2.2. Optical parametric oscillators

Basics

In DFG, the signal beam is amplified at the expense of the pump beam, according to the law of energy conservation (Eq.1) – annihilation of a pump photon leads to generation of one signal photon and one idler photon. This parametric amplification is the key to optical parametric oscillator (OPO), which is schematically pictured in Fig. 6. Unlike in DFG, the OPO has just one input beam. An optical resonator, or cavity, is built around the nonlinear crystal in order to amplify the signal beam, which initially arises from quantum noise [11]. The parametric oscillation starts if the pump power is sufficiently high, so that the parametric gain at the signal wavelength exceeds the round-trip losses of the resonator. This threshold pump power is of the order of 1 W for an optimized CW singly-resonant OPO (SRO) [47]. Here, the term singly-resonant refers to the case where only one of the beams, typically the signal beam, resonates in the OPO cavity. The threshold power, and hence the power requirement for the pump laser, can be significantly reduced by designing the cavity such that two waves (s and i) are resonant (doubly-resonant OPO, DRO) or three waves (p, s, i) are resonant (triply-resonant OPO, TRO) [11,48]. However, continuous wavelength tuning of DROs and TROs is complex compared to SROs [49], which is why SRO is by far the most widely used solution in molecular spectroscopy. Another solution, which has to some extent been used for molecular spectroscopy, is pump-enhanced SRO [50]. As the name implies, this is an SRO but the pump power is enhanced by a resonator, which can be either the same as the signal-wave resonator or a separate pump power build-up resonator.

An example of how the idler output power of a CW mid-infrared SRO depends on the pump power is shown in Fig. 7.

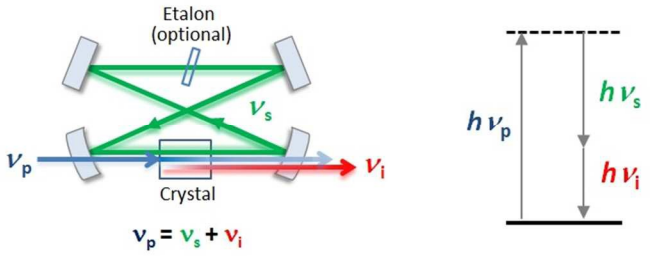

Figure 6. The principle of the singly-resonant OPO. The pump beam is focused into a nonlinear crystal, which is placed in a cavity formed by mirrors that are highly reflective for the signal beam. One signal and one idler photon is created when a pump photon is annihilated. An optional optical etalon can be used in the OPO cavity to enhance wavelength stability and tuning (see text for details).

The efficiency of the process can be really high: the pump depletion can exceed 90%, indicating that almost all pump photons are consumed [51,52]. This is one of the advantages of the SRO – the mid-infrared output power can be up to several watts, compared to a maximum of a few tens of milliwatts that can be obtained by DFG with high-power pump lasers.

In general, the OPO is in many ways similar to DFG. Both processes fulfil the same basic conditions, the law of energy conservation and the phase matching condition (Eqs. 1 and 2, respectively). Also the phase matching techniques and crystal materials are the same. The main difference in the practical implementation of these two methods is that the OPO requires an optical resonator. The resonator design typically starts by finding the optimum focusing, which follows the same rule as in DFG: The pump and signal beams should overlap in the nonlinear crystal, and have the same focusing of approximately $\xi = 1$. The size of the pump beam focus in the crystal is determined by the pump focusing optics outside the OPO resonator. The signal spot size in the crystal, on the other hand, is given by the resonator. The most common SRO resonator design is a folded (bow-tie) ring resonator [51], which is depicted in Fig. 6. The bow-tie resonator comprises two plane mirrors and two concave mirrors. The resonator design process is reviewed briefly in [52] and discussed in more detail, e.g., in [11,53]. In the case of an SRO, the resonator mirrors are highly reflective ($R > 99.5\%$) for the signal wavelength, but transmit the pump and idler wavelengths. The end facets of the nonlinear crystal should have good antireflection coatings for the resonant wavelength (residual reflectivity $R < 0.5\%$ or so) in order to minimize the optical losses that would lead to an unintentionally high oscillation threshold. In practice, a threshold of ~1 W can be obtained with total round-trip losses of about 2% using a 5-cm long MgO:PPLN crystal [48].

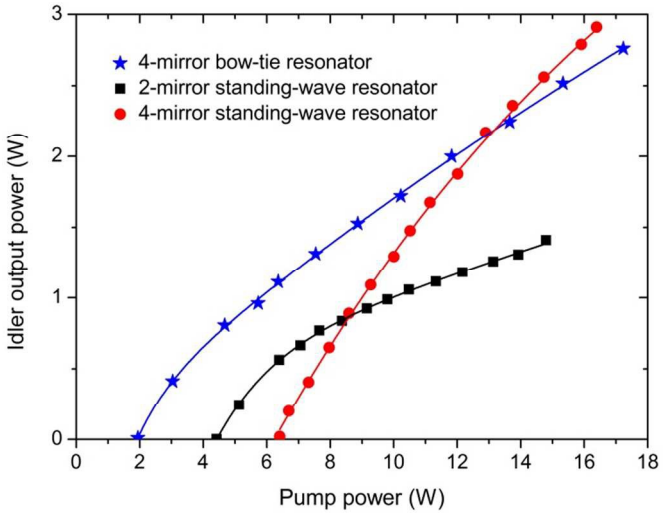

Figure 7. Mid-infrared output power as a function of pump power for three different CW SRO cavity configurations [58]. The pump wavelength is 1064 nm and the mid-infrared idler wavelength is 3100 nm. The pump power was measured before the SRO cavity. The output powers were measured after dichroic optics that separates the mid-infrared beam from the pump and signal beams.

Wavelength stability

In the case of DFG, the stability of the mid-infrared idler wavelength is fully determined by the stability of the pump and signal laser (Eq. 1). In OPOs, the wavelength stability is significantly affected by the OPO cavity, in which the signal beam resonates. As already discussed in the context of DFG, the parametric gain profile of, e.g., PPLN in mid-infrared generation is typically broad, up to several hundred GHz (Fig. 4). As a result, the CW OPOs are prone to mode hops: The resonant signal frequency can jump from one longitudinal mode of the resonator to another, because the mode spacing (free spectral range, *FSR*) of the resonator is typically small compared to the width of the parametric gain profile [52]. This is exemplified in Fig. 8. Recall that any jump in the signal frequency is immediately seen as a jump in the mid-infrared idler frequency, according to Eq. 1.

The probability of mode hopping is increased by environmental disturbances, such as air flows, mechanical vibrations, and temperature variations [52,54]. C.R. Phillips and M. Fejer have also that modulation instability plays an important role in CW SROs [55]. One of the findings of their research is that there is a maximum power level at which the SRO can remain stable – above the instability threshold mode hops and multimode oscillation are expected. Moreover, this instability threshold, and hence the maximum output power of stable SRO operation, depends on the wavelength. This is illustrated in Fig. 9 for the most commonly used mid-infrared CW SRO – the one that is pumped at 1064 nm and uses a MgO:PPLN crystal as the nonlinear material. At high intracavity power levels of several hundred watts, stable single-mode operation of an SRO can also be compromised by other effects, such as stimulated Raman oscillation and secondary (cascaded) optical parametric oscillation [52,56,57].

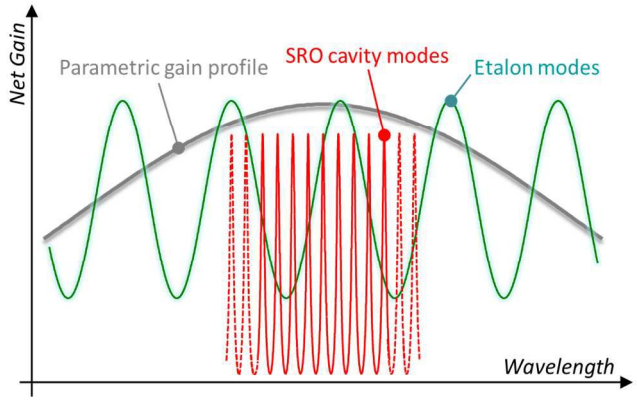

Figure 8. Wavelength selection in a mid-infrared singly-resonant OPO. The FWHM of the parametric gain profile is typically ~10 cm^{-1} (300 GHz), depending on the wavelength and the crystal material. The cavity mode spacing is much smaller, of the order of 0.01 cm^{-1} (300 MHz). Hops between the cavity modes can be suppressed by using, e.g., an intracavity etalon as a frequency selective element (see text for details).

Below the instability threshold (Fig. 9), stable mode-hop-free operation for several hours can be achieved by mechanical vibration isolation (optical table), by good control of the SRO/crystal temperature, and by covering the SRO cavity so that it is not exposed to air flows [50,58,59], see Fig. 10. In particular, good stabilization of the temperature of the nonlinear crystal (with a precision of ~10 mK) is essential for stable mode-hop-free operation [52,54]. It has also been shown that the photorefractive effect, as well as heating of the crystal due to residual absorption of the resonant beam can have a significant effect on the SRO stability, although quantified information on the role of these effects is scarce [52,60,61]. Thermal load in the nonlinear crystal can be alleviated by reducing the intracavity power, in practice by using a partially reflective cavity mirror or another component that couples out a few percent of the resonating beam [51,56,62,63]. Such output coupling also increases the SRO instability threshold, which makes it possible to reach very high single-mode output powers if only a high power pump laser is available [55,64,65,66]. The reduction of thermal load and other effects arising from high intracavity power is also usually beneficial for the output beam quality [62], although thermal waveguiding due to strong thermal lensing in the crystal can also lead to a high beam quality if the cavity dimensions are chosen properly [67]. Spatial distortion of the output beam can also be caused by the photorefractive effect. The photorefractive effect can be reduced by using, e.g., an MgO-doped PPLN crystal and by keeping the crystal temperature constant [68].

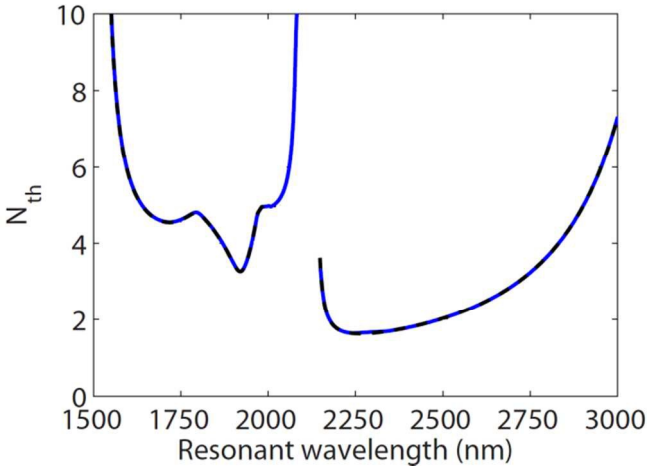

Figure 9. Calculated instability threshold N_{th} versus the resonant (signal) wavelength for an SRO pumped at 1064 nm [55]. The nonlinear gain material is a 5 cm long PPLN crystal, and the round-trip power loss of the resonant wave is 1%. N_{th} is defined as the lowest pump power for which the SRO becomes unstable, divided by the oscillation threshold power. Reproduced with permission from [55].

Several methods have been developed to suppress mode hops even when operating the instrument in more challenging conditions, outside of research laboratories. The most common of these methods is to use an intracavity etalon, which produces periodic wavelength-dependent losses, hence reducing the probability of mode-hops to nearby cavity modes [51,54,60]. The principle of this method is illustrated in Fig. 8. The etalon mode spacing should be chosen so that modulation instability peaks are properly suppressed [55]. Otherwise so-called etalon mode hops, i.e. hops to the adjacent etalon transmission modes, can occur [69]. In addition to etalons, also other frequency

selective optical elements can be used to suppress mode hops. The main challenge is to keep the losses for the resonant mode low enough, typically below a few %, in order to avoid the increase of pump threshold impractically high [69]. This requirement can be met with high-efficiency diffraction gratings [70,71] or Bragg gratings [66,71,72]. The advantage of using a grating instead of an etalon is that the grating only has one maximum, which avoids the problem of etalon mode hops. This feature is particularly important if the SRO needs to be operated close to the signal-idler degeneracy wavelength, where the bandwidth of parametric gain, and hence the mode-hop probability, becomes exceptionally large [73,74].

In addition to the passive SRO stabilization and control methods (temperature stabilization, etalons, gratings), also active methods have been used. In practice, this means that the frequency of the SRO signal or idler beam is locked to an external reference, which can be an atomic or molecular absorption line [25,59], a stable high-finesse cavity [75,76,77,78], an optical frequency standard [79], or an optical frequency comb [59,80,81,82,83]. With these methods, it is possible to stabilize and control the SRO frequency at the MHz level or better, although at the cost of increased system complexity. The linewidth of the SRO can be narrowed down to the kHz level relative to the reference [76,78,79].

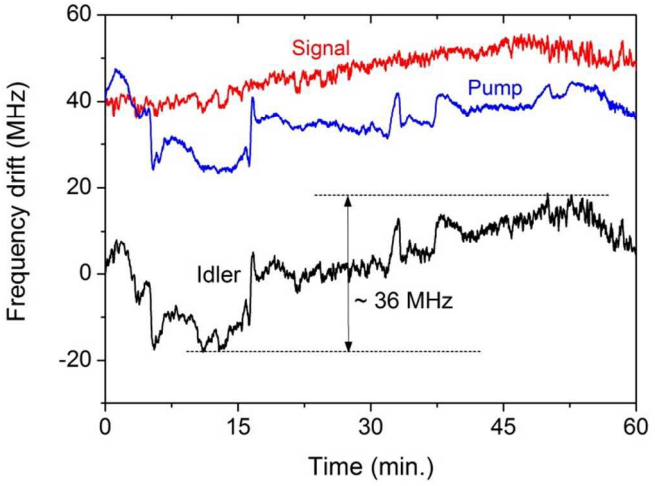

Figure 10. The black solid line shows mode-hop-free idler frequency drift of a free-running SRO over an hour. The SRO was pumped with an amplified Yb-fibre laser at 1.064 µm, and the idler wavelength was 3.39 µm [59]. The contributions of pump and signal drifts are also shown, with an offset of 40 MHz that has been added for clarity. The SRO was operated in a temperature stabilized laboratory [73]. Temperature of the PPLN crystal was stabilized with a precision better than 10 mK. If the SRO cavity is exposed to air flows, or if the temperature instability of the PPLN crystal is > 100 mK, the signal (and idler) frequency fluctuations typically exceed 100 MHz, and mode hops appear frequently (see, e.g., [54]).

Wavelength tuning

The coarse wavelength tuning range of an OPO is practically independent of the pump laser tuning range. The idler wavelength can be calculated from the phase-matching condition just like in the case of DFG (Fig. 5), but now the signal wavelength generated in the OPO automatically adjusts so that the phase-matching condition $\Delta k = 0$ is fulfilled. This means that coarse wavelength tuning can be done simply by varying the crystal temperature and/or QPM period, as is exemplified in Fig. 5 – the pump wavelength can be fixed. The wavelength tuning range is often limited by the range of the OPO cavity mirrors, but a tuning range of several hundred nanometres can be achieved around 3 µm without replacing the mirrors or other components [57,60,84]. In practice, such coarse tuning is not continuous, but the OPO signal frequency hops from one cavity mode to another [69], leading to equally large jumps in the idler frequency. The magnitude of a mode hop is typically several GHz, which makes this tuning method unsuitable for high-resolution spectroscopy. This problem can be avoided by using a continuously tuneable pump laser: Just like in the case of DFG, any change in the pump frequency is completely transferred to tuning of the idler frequency if the signal frequency remains fixed. This works as long as the pump tuning range is small compared to the parametric gain bandwidth.

The use of an intracavity etalon or grating gives an additional tool for wavelength control: the frequency of highest overall gain can be varied by varying the etalon (or grating) angle. Tuning by these two methods is exemplified in Fig. 11. In brief, a CW SRO of this type is used for molecular spectroscopy as follows:

(1) The SRO wavelength is first coarsely set to the desired range by adjusting the temperature and/or QPM period of the crystal.

(2) The etalon (or grating) is subsequently used to set the oscillation wavelength with a typical precision of 10 to 100 GHz.

(3) Finally, fine scanning over the molecular absorption lines is done by scanning the pump laser.

This wavelength scanning procedure can be automatized, as demonstrated in Refs. [60,85].

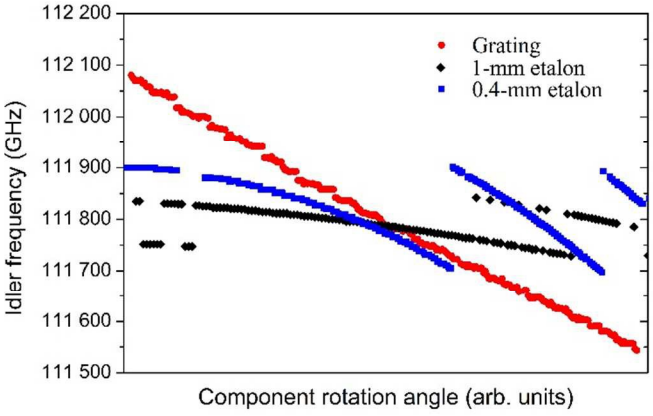

Figure 11. Wavelength tuning of an SRO by intracavity etalon, as well as by grating, which replaces one of the cavity mirrors [70]. Tuning with two different etalons, one 0.4 mm thick and another 1 mm thick, is shown. Both etalons are solid YAG plates. Etalon rotation eventually leads to an etalon mode hop, while the grating allows monotonic tuning within the parametric gain curve.

The mode-hop-free tuning range of a modern SRO pump laser can be from a few GHz up to several THz, so etalon angle tuning is not necessarily needed in the scanning process. In fact, wavelength tuning can be entirely done using the pump tuning, in case a broadly tuneable pump laser is available. Such pump scanning over hundreds of nanometres is illustrated in Fig. 12. A CW Ti:sapphire laser was used as a pump laser, and the scanning was done by adjusting the pump laser wavelength while keeping all other parameters, including crystal temperature and QPM period, constant [84]. This tuning method is simple and fast, but requires a widely tuneable high-power pump laser. Note that the mode-hop-free scan range of the OPO is the same as that of the pump laser (40 GHz). For large scans, the signal wavelength of the OPO follows the pump wavelength scanning so that the phase-matching condition remains fulfilled (Fig. 12).

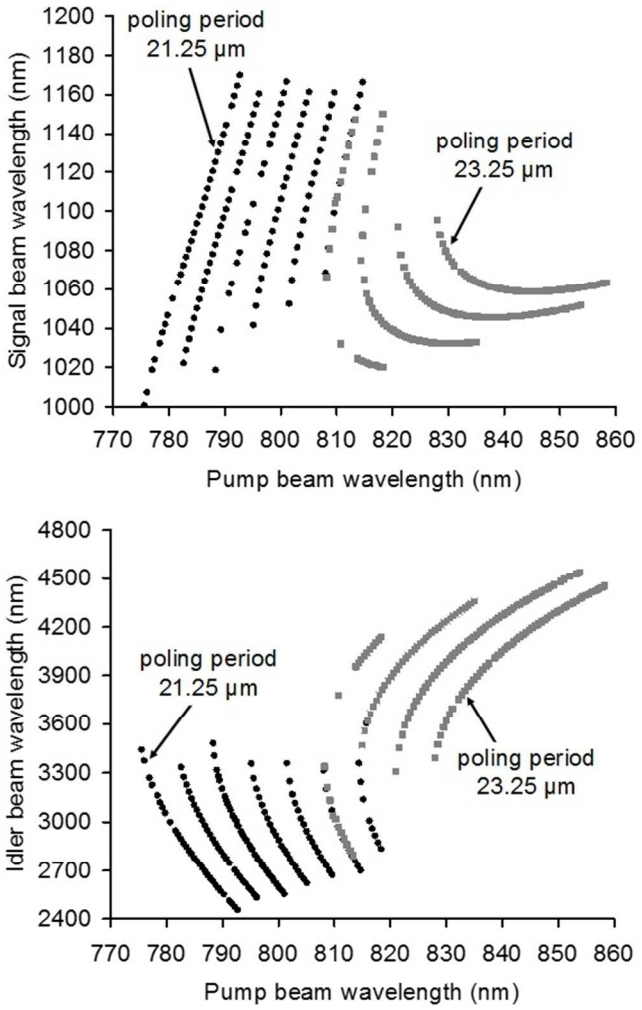

Figure 12. Lower panel: Idler wavelength tuning of a mid-infrared SRO by tuning the pump laser (Ti:sapphire laser) wavelength. The tuning is shown for two different QPM periods of the PPLN crystal, which was used as the nonlinear material. The crystal temperature was fixed to 320 K. The upper panel shows how the resonant signal wavelength follows the tuning according to Eq. 1. Reproduced with permission from [84].

Typical implementations

The first singly resonant CW mid-infrared OPO based on PPLN was demonstrated by Bosenberg *et al*. in 1996 [51]. The OPO was pumped with a multimode 13.5 W Nd:YAG laser at 1064 nm, the signal wave resonated at ~1.5 µm, and the mid-infrared output was provided at > 3 µm wavelength. The OPO cavity design was the same as shown in Fig. 6, and an intracavity etalon was used to reduce the number of mode hops and to facilitate frequency tuning. This same CW SRO design is still used in most implementations designed for molecular spectroscopy, including the most common commercially available instruments. Also, the figures of merit of the first instrument, the maximum mid-infrared output power (3.55 W), pump depletion (93%), and wavelength tuning range (3.3 to 3.9 µm), are comparable to what is obtained with a typical instrument of today.

The main technological advance related to CW SROs since 1996 has been the development of high-power (multiwatt) *narrow-linewidth* (single longitudinal mode) CW pump laser systems based on solid-state lasers [60,86], as well as on Yb-doped fibre amplifiers [47,87]. In practice, the maximum mid-infrared output power of a CW SRO based on MgO:PPLN is limited to approximately 10 W by the damage threshold of the crystal [66]. The high available pump power has also made it possible to operate MgO:PPLN-based CW SROs at wavelengths as long as 5.4 µm, although the output power drops to a few milliwatts due to the strong absorption in lithium niobate at wavelengths longer than ~5 µm [57,86].

The Yb-fibre amplifier is usually seeded either with an Yb-fibre laser or a semiconductor diode laser that operates at approximately 1.06 µm. A fibre laser has a narrow instantaneous linewidth (<100 kHz), good frequency stability (drift <100 MHz/h), and can be tuned up to ~100 GHz without mode hops by stretching the fibre with a piezoelectric actuator or a heater. A diode laser, which is typically a distributed-feedback (DFB) laser, a distributed-Bragg-reflector (DBR) laser, or an external-cavity diode laser (ECDL) often possess a larger linewidth (1 MHz) than the fibre lasers. On the other hand, the diode laser frequency can be modulated at several hundred MHz, which is useful in certain spectroscopy methods, such as frequency-modulation spectroscopy. The mode-hop-free tuning range of the DFB and DBR diode lasers is typically a few tens of GHz, but an ECDL can be scanned up to several THz, which has proven useful in molecular spectroscopy [77,88,89]. Mode-hop-free SRO scanning speeds of several THz/s have been reported with both DBR lasers [90,91,92] and ECDLs [88].

Another improvement since the first demonstration of a CW SRO is that MgO:PPLN crystals have replaced undoped PPLN as the standard nonlinear gain material. This has made it possible to operate the crystal even at room temperature, while undoped PPLN needs to be heated to > 370 K in order to avoid photorefractive damage [60]. Also, fan-out crystals are available, making coarse wavelength tuning easier and faster, since the tuning can be done by mechanical translation of the crystal, while keeping the temperature constant [93]. Note that

the temperature tuning method is slow, since a couple of minutes are typically required for the OPO to stabilize after stepping the crystal temperature [52].

EMERGING TECHNOLOGIES

The development of high-power (several watts) CW pump lasers during the past decade has been a key factor to the development of the CW SROs that are suitable for high-resolution spectroscopy in the mid-infrared region. While these instruments are excellent for laboratory use, the relatively high power consumption can be an issue in field applications. As mentioned before, the pump power requirement can be somewhat reduced by using a pump-enhancement cavity [50]. Even lower threshold powers can be achieved with DROs and TROs. However, continuous wavelength tuning of these OPOs is challenging [49], which has precluded their use in molecular spectroscopy, apart from some demonstrations in the near-infrared region [80].

Recently, so-called hybrid OPOs with significantly reduced threshold powers have been reported. In a hybrid OPO, the threshold is reduced by providing additional optical gain to the resonating signal beam by an additional laser gain element, which can be a doped crystal [94] or a semiconductor gain mirror [95]. These hybrid OPOs are presumably suitable for spectroscopic applications, although experimental proofs of the applicability have not been reported yet.

Another recently developed CW mid-infrared OPO is based on a whispering gallery mode resonator, which is fabricated from a nonlinear crystal material, such as lithium niobate [48]. Either birefringent phase matching or quasi-phase matching can be used, and the oscillation threshold can be as low as a few microwatts. The problem is that these OPOs are triply resonant, which together with thermal issues makes large continuous wavelength tuning, and hence trace gas spectroscopy, challenging [96]. One of the benefits of the whispering-gallery-mode resonators is compactness – the resonator diameter is typically a few millimetres, while a conventional bulk OPO has a size of a shoebox. On the other hand, a monolithic CW-pumped high-power SRO has also been demonstrated. The SRO cavity was formed in a 5-cm long PPLN bulk by applying a spherical polish and a highly reflective coating to two of the facets of the crystal and using total internal reflection on one side of the crystal [97].

Finally, a promising route towards inexpensive, robust, and field-applicable mid-infrared parametric generation is to build a CW OPO around a waveguide crystal [98,99]. Continuous-wave operation of an idler-resonant mid-infrared SRO with near-subharmonic 1560-nm pumping has already been demonstrated with a low-loss Ti:PPLN waveguide [98]. The authors reported a low threshold power of 275 mW, as well as a total output power (signal + idler) of 300 mW with 1.25 W pump power. The total wavelength tuning range (signal + idler) of the device extends from 2.8 to 3.5 μm. Interestingly, the tuning can be done simply by changing the pump laser wavelength, which also allows for continuous scanning of the non-resonant signal frequency over several GHz, making the device potentially useful for molecular spectroscopy.

2.3. Mid-infrared frequency combs

An optical frequency comb (OFC), or a laser frequency comb, has a broadband spectrum that consists of a large number of discrete, equidistant lines [100]. An example of an OFC spectrum is schematically shown in Fig. 13. The frequency of each line, or tooth, can be written as

$$f_m = f_{ceo} + mf_r, \quad (8)$$

where $f_{ceo} < f_r$ is the carrier-envelope offset frequency, and f_r is the repetition frequency, i.e., the mode spacing of the comb in the frequency domain. Mode number is denoted by the integer m. The repetition frequency of an OFC useful for high-resolution molecular spectroscopy is typically of the order of 100 MHz. (The repetition frequency is determined by the round-trip length L_{rt} of the laser cavity: $f_r = c/L_{rt}$). The frequency comb is fully stabilized if both f_{ceo} and f_r are locked to an accurate frequency reference, such as an atomic clock. The stabilization of f_r is relatively simple, because the ~100 MHz beat-note frequency between adjacent comb teeth can easily be measured, and the repetition frequency can be controlled by adjusting the cavity length of the comb generator. The most common method for f_{ceo} stabilization relies on so-called f-2f interferometer, which requires an octave-spanning comb – in other words a comb whose mode at the low-frequency end of the spectrum can be directly compared with a mode at the high-frequency end after optical frequency doubling. The principle of this method is depicted in Fig. 13.

The most widely used method for OFC generation is based on mode-locked femtosecond lasers. The relationship between the time- and frequency domain representations of a mode-locked laser output is given by the Fourier transform (Fig. 13). In the time domain, a mode-locked laser produces short pulses at a repetition rate that equals to the comb mode spacing – the repetition frequency – in the frequency domain. The carrier-envelop offset frequency arises, as the name implies, because in general the relative phases of the pulse carrier and envelope change from pulse to pulse.

The fully-stabilised OFC based on mode-locked laser was discovered in 1999 and has since been used, among other applications, for direct frequency comb spectroscopy [100]. The power of this method can be intuitively understood by noticing that an OFC spectrum essentially corresponds to a large number of parallel continuous-wave laser spectra. The number of these modes can be up to a million; therefore a large number of molecular absorption lines and species can be spectroscopically measured simultaneously. Unfortunately, the extension of the frequency comb technology to the mid-infrared fingerprint region has proven difficult – direct OFC generation with mode-locked lasers at wavelengths longer than ~2.5 μm is yet to be demonstrated [101]. This problem can be solved by transferring an OFC from the near-infrared to the mid-infrared

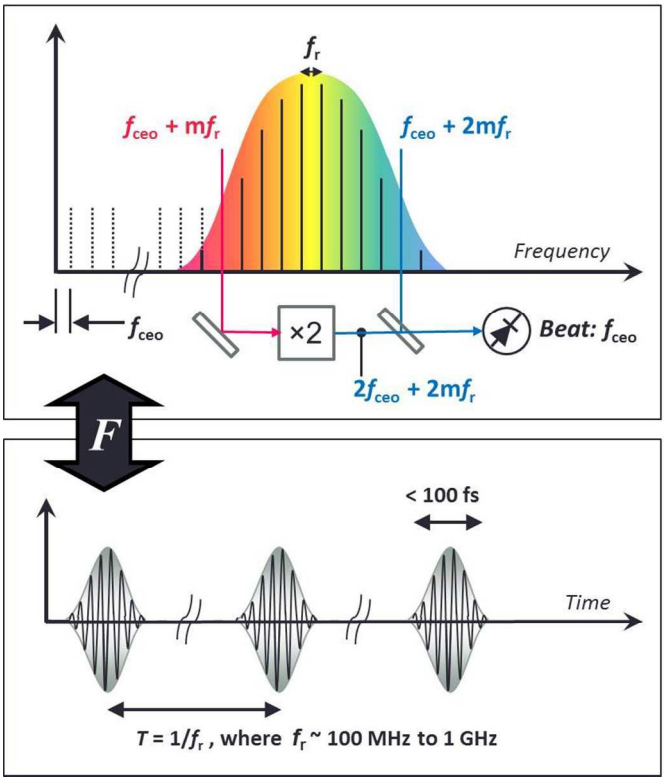

Figure 13. *Upper panel:* Schematic representation of the spectrum of an optical frequency comb. The comb mode spacing is exaggerated for clarity – a typical mode spacing, or repetition frequency, is 100 MHz, while the comb can exceed over 100 THz, hence consisting of approximately a million modes. The principle of f_{ceo} counting is also shown. *Lower panel*: Time domain representation of a mode-locked laser frequency comb.

by nonlinear optics, using either an OPO or DFG, as is explained in the following.

SYNCHRONOUSLY PUMPED PARAMETRIC OSCILLATORS

The basic principle of a synchronously pumped OPO (SP-OPO) is the same as that of a CW OPO (Fig. 6). The main difference is that the synchronously pumped OPO is pumped by short (< 500 fs) pulses produced by a mode-locked near-infrared laser. Due to the shortness of these pulses, the SP-OPO cavity length needs to be matched (synchronized) with that of the mode-locked pump laser – otherwise the subsequent pump pulses would not overlap in the nonlinear crystal with the parametrically generated pulses propagating in the SP-OPO cavity [102,103,104]. A typical 30-fs pulse from a mode-locked Ti:sapphire laser has a spatial length of ~9 μm in air (c×30 fs), which gives an idea of the required level of synchronization. If the pump spectrum is a frequency comb, the signal and idler spectra are also combs, according to the law of energy conservation (Eq. 1). The repetition frequency is typically the same as that of the pump laser, although a fractional- or multiple-length cavity can be used to multiply the repetition frequency of the pump [105,106].

A good introduction to general aspects and recent developments of frequency combs based on SP-OPOs can be found in Ref. [107]. Here, we focus on features relevant for high-resolution spectroscopy applications. As mentioned, doubly-resonant continuous-wave OPOs are not usually used in spectroscopy, because of the difficulties with frequency stabilization and tuning. With synchronously pumped OPOs, however, the doubly-resonant scheme is particularly favourable: In the special case of a degenerate SP-OPO, the signal and idler spectra overlap. The modes of the two lock to each other via mutual injection locking, producing a stable, phase-locked output where the signal and idler spectra are indistinguishable, as has been demonstrated by Vodopyanov and co-workers [103,108]. In this case, the offset frequency f_{ceo} of the signal/idler comb automatically locks to that of the pump comb, while in a singly-resonant SP-OPO the f_{ceo} of the mid-infrared comb needs to be stabilized separately [102,109]. An additional advantage of the degenerate, doubly-resonant SP-OPO scheme is that at degeneracy the phase-matching bandwidth is broad. The gain bandwidth is further broadened by the possibility of using a short nonlinear crystal (1 mm or less), owing to the low threshold power of a doubly resonant OPO. In practice, an octave-spanning optical output spectrum – much wider than the pump spectrum – can be obtained with a short nonlinear crystal, see Fig. 14 [110]. The degenerate (subharmonic) synchronously pumped DROs have so far been used to produce broadband mid-infrared combs at 2.5 to 3.8 μm (Er-fibre laser pumping at 1560 nm, 200-μm-long MgO:PPLN crystal) [103], at ~4.4–5.4 μm (Cr^{2+}:ZnSe- or Cr^{2+}:ZnS-laser pumping at ~2.4 μm, 500-μm-long orientation patterned GaAs crystal) [111,112], and at 2.6 to 6.1 μm (Tm-fibre laser pumping at 2050 nm, 500-μm-long orientation patterned GaAs crystal) [110]. The need for a pump laser at the second harmonic of the intended mid-infrared centre frequency can be alleviated by using cascaded pumping. As an example, Marandi *et al*. have demonstrated broadband comb operation at ~4 μm starting from a commercially available 1 μm femtosecond pump laser [113]. Typical mid-infrared output powers of the comb generators based on synchronously-pumped degenerate DROs are a few tens of milliwatts, which is sufficient for most spectroscopy applications.

Mid-infrared OFC sources based on singly-resonant SP-OPOs have also been reported. These SP-SROs can produce watt-level output powers [102] but the instantaneous spectral width is smaller than that of synchronously pumped DROs, typically ~10% of the comb centre wavelength [102,104]. On the other hand, the centre wavelength of a SP-SRO can be scanned the same way as that of a CW SRO – typically by varying the QPM period [102], the SP-SRO cavity length [104,114], or pump wavelength [115]. As an example, a phase-stabilized comb tunable from 2.8 to 4.8 μm has been demonstrated by Ye's group with a 7-mm long MgO:PPLN fan-out crystal and Yb-fibre laser pumping at 1070 nm [102]. Phase stabilization was in this case realized by utilizing parasitic mixing of the pump, signal, and idler beams in the nonlinear crystal, such that the signal and idler combs could be referenced to the pump comb. In a recent experiment of Reid's group, the nonlinear crystal (multigrating PPKTP) was specifically designed for efficient mixing of the pump and idler

beams, in order to enable convenient stabilization of the mid-infrared comb over its entire tuning range, from 1.95 to 4.0 μm [114].

If the SP-OPO cavity dispersion owing to a relatively long crystal is large enough, it is possible to pump a SP-OPO with two pump lasers that have slightly different repetition rates [116]. Another possibility is to use a two-crystal SP-OPO, where each crystal is independently pumped with a femtosecond laser [117]. Such SP-OPOs that simultaneously produce two mid-infrared frequency combs are useful for dual-comb spectroscopy [118,119].

A common method for spectral broadening (supercontinuum generation) of mode-locked laser light in the near-infrared region is to pass the light through a highly nonlinear optical fibre [100]. This method has recently become available also in the mid-infrared region [120]: Spectral broadening of mid-infrared combs has been demonstrated in tapered chalcogenide fibres at 1-3.7 μm [121] and at 2.2-5 μm [122]. Considerable spectral broadening can also been achieved in optical waveguides, such as in a nanospike chalcogenide waveguide at 3-6 μm (discontinuous) [123], or in a silicon nanophotonic wire waveguide at 1.5-3.3 μm [124]. An octave spanning spectrum has been produced in a $LiNbO_3$ waveguide pumped by a Tm-doped fibre laser system [125].

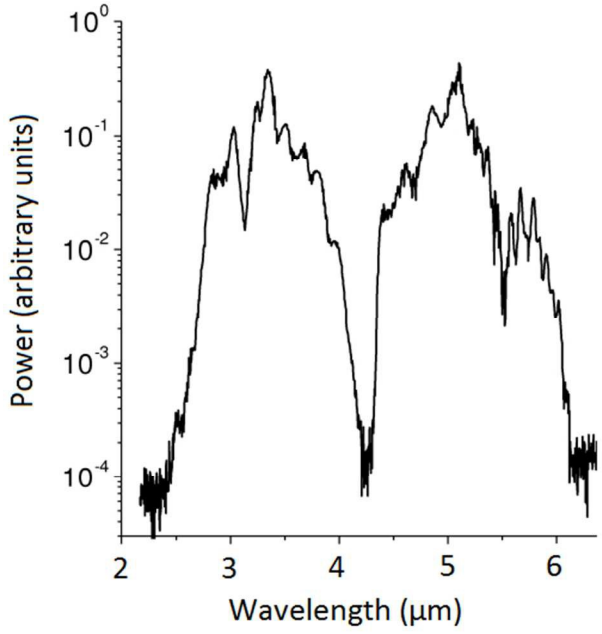

Figure 14. The spectrum of an octave spanning mid-infrared frequency comb generated by a degenerate, synchronously pumped OPO. Note that individual modes of the comb are not resolved due to the limited resolution of the optical spectrum analyser. The large dip in the measured spectrum at ~4.2 μm is due to CO_2 absorption in air between the OPO and spectrum analyser. Reproduced with permission from [110].

MID-INFRARED COMB GENERATION BY DFG

In addition to parametric oscillation, a near-infrared frequency comb can be transferred to the mid-infrared region by difference frequency generation. The simplest implementation of this approach is to mix a near-infrared comb with a CW laser beam in a nonlinear crystal. As an example, a 180-nm wide comb tuneable from 2.9 to 3.5 μm has been generated by mixing an amplified near-infrared (1.5 μm) frequency comb with pump light generated by an Yb-fibre amplified ECDL (1030-1070 nm) in a PPLN crystal [126]. The mid-infrared comb was referenced to the SI primary standard by phase-locking the pump laser to the near-infrared comb, which was fully stabilized and extended down to ~1 μm wavelength. The main limitation of this method is low mid-infrared output power, typically a few microwatts in total, or ~100 pW/comb tooth. A higher power level of approximately 0.5 mW (1 μW/tooth) has been achieved by difference frequency mixing inside a laser cavity in order to increase the pump power in the nonlinear crystal [127]. In this case, the pump laser was a Ti:sapphire laser operating at ~0.8 μm, and the near-infrared comb was produced by an Yb-fibre laser system at 0.5-1.1 μm.

Because the DFG efficiency is proportional to the peak powers of the input beams, a high-power mid-infrared comb by DFG can be achieved by mixing two branches of a femtosecond comb instead of mixing a comb with a CW laser [128]. As an example, an average power of more than 500 mW (3 μW/mode) was recently achieved between 2.8 and 3.5 μm using this method [129]. Neely *et al*. have generated a 125 mW comb tuneable from 3 to 4.4 μm by mixing, in MgO:PPLN, the beam of a femtosecond Yb-fibre laser and a Raman-shifted soliton generated with the same laser [130]. The same approach has also been used with other crystal materials, such as GaSe, $AgGaSe_2$, and QPM GaAs, allowing for large tuning ranges from 3 μm to 10 μm or beyond [131,132,133]. Recent studies have shown that the mid-infrared power can be boosted to the watt-level by using multi-stage optical parametric amplification [134].

EMERGING TECHNOLOGIES

The longest wavelength that has so far been directly obtained from a mode-locked laser is 2.8 μm, which has been demonstrated with an Er-doped ZBLAN laser [135]. A more common solution for operation at ~2.5 μm is to use Cr^{2+}:ZnSe and Cr^{2+}:ZnS lasers [101]. Mode-locked mid-infrared lasers are also being developed based on, e.g., Tm^{3+}, Ho^{3+}, and Fe^{2+} doped crystals, as well as on quantum cascade lasers [136]. Despite the recent progress in the research of mode-locked infrared lasers, the most promising new methods for mid-infrared comb generation are still based on parametric frequency conversion [101].

Difference frequency generation and optical parametric oscillation discussed above are examples of quadratic nonlinear processes that arise from the second order susceptibility ($\chi^{(2)}$) of the nonlinear material. An optical frequency comb can also be generated in a cubic ($\chi^{(3)}$) nonlinear material, via optical Kerr effect that leads to spectral broadening of a CW pump laser beam. This so-called Kerr comb generation was first demonstrated in 2007 using SiO_2 microresonators, and has since been realized with several other materials [137]. Kerr combs at wavelengths longer than 2.5 μm have recently been reported using, at least, silicon [138], CaF_2 [139], and MgF_2

[139,140]. In general, the Kerr comb generation requires the use of a microresonator, which leads to a large mode spacing of > 10 GHz, rendering these combs unsuitable for high-resolution multispecies trace gas spectroscopy. A potential solution to this problem is based on cascaded quadratic nonlinearity, which mimics the cubic nonlinearity. The cascaded quadratic effect leads to strong self-phase modulation and four-wave mixing even in bulk systems [125], and can be used to generate combs with ~100 MHz to 1 GHz mode spacing [141,142,143,144]. This method, in combination with intracavity DFG, has already been used to produce a high power (> 3 W) mid-infrared comb tunable from 3 to 3.4 μm [145]. The main challenge with this new type of frequency comb is the excessive phase and amplitude noise observed in the first prototype systems – further research is needed in order to achieve low-noise operation, which is a prerequisite for accurate and sensitive OFC spectroscopy.

3. Applications

In the following, we review some of the most important applications of tuneable single-frequency mid-infrared OPOs and difference-frequency generators, as well as parametric frequency combs. We first discuss trace gas detection, which is one of the most important uses of mid-infrared spectroscopy, and has several existing and potential applications. Industrial process control and environmental monitoring are examples of applications where these methods have already proven useful in the field [1]. Medical diagnostics by analysis of exhaled breath is also developing rapidly, with several demonstrations in laboratory conditions [2,146].

In addition to trace gas detection, we discuss the use of parametric mid-infrared sources in fundamental research of molecules. We have selected a bunch of examples that illustrate not only the diversity of applications, but also the wide variety of spectroscopic methods that can be combined with the mid-infrared sources presented in Section 2.

3.1. Trace gas detection

Several demonstrations of trace gas detection by mid-infrared DFG-sources and OPOs have been reported during the past 20 years. The first reports of high-resolution trace gas detection by CW DFG were published in the beginning of 1990's. The first setups were based on bulky dye lasers and Ti:sapphire lasers [14], but soon more compact spectrometers based on tunable diode lasers, fibre lasers, and PPLN crystals were developed [147,148,149]. The advent of PPLN, as well as high-power solid state lasers and fibre lasers, lead to the development of single-mode CW OPOs in the beginning of 2000s, further increasing the mid-infrared power as compared to the DFG-based systems [150].

Direct absorption spectroscopy (DAS), in which the mid-infrared beam is passed through the gas sample and then detected with a photodetector, is the simplest method for trace gas analysis using both DFG and OPO. With high enough mid-infrared power for nearly shot-noise-limited detection (~0.1 mW depending on the detector), a normalized noise-equivalent absorption coefficient (NNEA*) as small as 10^{-6} to 10^{-8} $cm^{-1}Hz^{-1/2}$ can be obtained, especially if balanced detection etc. is used to compensate for the noise caused by power fluctuations of the light source [151,152,153,154]. When used for spectroscopy of strong fundamental vibrational transitions of molecules like CH_4 and N_2O within the atmospheric window between 3 and 5 μm (Fig. 1), this translates into a detection limit of ~1 ppm (parts-per-million) volume-mixing ratio with a typical absorption path length of 1 m. An obvious solution to improve the sensitivity of trace gas detection is to increase the absorption path length. Apart from certain applications in atmospheric monitoring [155], increase of the path length simply by placing the detector far away from the light source is impractical. A common approach to achieve a path length of up to a couple hundred meters is to use a multipass cell. Multipass cells of, e.g., Herriot or White type, are commonly used in the mid-infrared region, as they can be implemented using metal coated mirrors [1,151]. The spectrometers based on multipass cells are relatively simple, compact, and robust, and hence suitable for field applications of trace gas detection. As an example, a 3.3-μm DFG source combined with a 80-m Herriot cell has been used to detect CH_4 in air with a sub-ppb detection sensitivity (corresponding to NNEA ~ 5×10^{-10} $cm^{-1}Hz^{-1/2}$) [154]. Other compounds measured in air with similar setups and with essentially similar performances include CO (5 ppb), N_2O (2 ppb), CO_2 (100 ppb) [156], as well as benzene (50 ppb) [157]. As usual, these measurements were carried out using a sample pressure lower than the atmospheric pressure, in order to reduce pressure broadening of the absorption lines and hence to improve the spectroscopic resolution and selectivity.

The high sensitivity and selectivity of CW mid-infrared laser spectroscopy are useful not only for trace gas detection, but also for the determination of isotopic compositions of trace gases. Accurate measurements of isotope abundance ratios are needed in several areas, including environmental and medical sciences. As an example, the measurement of temporal and local changes of $^{13}CO_2/^{12}CO_2$ can be used to locate and quantify CO_2 sinks and sources, such as volcanic sources and anthropogenic (industrial, agriculture) sources [158,159,160]. Reliable measurements of isotope ratios typically require a high spectroscopic resolution, owing to the spectral proximity of the absorption features of different isotopes and interfering species. A typical DFG-based high-resolution mid-infrared spectrometer can provide 10^{-3} -level precision in the determination of the isotope ratio for, e.g., CO_2 [158] and N_2O [159].

While the increase of absorption path length by use of a multipass cell aims at enhancement of the absorption signal, the spectrometer performance can also be improved by noise-reduction techniques, such as those based on modulation. The detection sensitivity of DAS can be improved by 2-3 orders of

* Normalized to a 1-cm absorption path length and 1 Hz (electric) detection bandwidth, which is inversely proportional to the integration time of a *single* data point [151].

magnitude by using wavelength modulation spectroscopy (WMS) or frequency modulation spectroscopy (FMS). In both of these techniques, the wavelength/frequency of the mid-infrared source is modulated at frequency f_{mod}, and the demodulation is done either at the modulation frequency f_{mod} or its harmonics ($2f_{mod}$, $3f_{mod}$,…). The main conceptual difference between WMS and FMS is that in WMS the modulation frequency f_{mod} is low compared to the half-width Δf_{HWHM} of the absorption line, while in FMS $f_{mod} > \Delta f_{HWHM}$. This leads to slightly different spectra of the demodulated signals in the two cases, and WMS and FMS are often discussed separately although they are essentially the same technique just applied in different frequency regimes [161].

Demodulation at $2f_{mod}$ is most commonly used in trace gas detection, because it gives the signal maximum on top of the absorption line, while the odd harmonics have zeros at absorption maxima [159,161]. Modulation of the wavelength can most easily be done by directly modulating the wavelength of the pump laser, as the modulation is transferred to the mid-infrared beam according to Eq. 1. While the diode-laser based pump sources can be modulated at very high frequencies, up to tens of GHz, the electrical bandwidths of mid-infrared detectors typically limit the usable range of f_{mod} to a few MHz or below. Techniques like two-tone FMS can be used to overcome this limitation [162], but in general mid-infrared trace gas spectroscopy utilizes the WMS regime rather than FMS. The improvement of the spectroscopic detection sensitivity in WMS is mainly due to reduced noise level, as the detection of the absorption signal is transferred from DC to a higher frequency. (In most cases the measurement noise is dominated at low frequencies by 1/*f*-noise). The high signal-to-noise ratio, together with the relative simplicity of the method, has made WMS one of the most popular approaches in the field applications of trace gas detection [148, 163]. For instance, a detection limit of 74 ppt (in 1 min.) for formaldehyde (H_2CO) has been achieved with a spectrometer that combines WMS with a multipass cell, and utilizes a 3.5-μm DFG source [163]. Demonstrations of WMS using CW mid-infrared OPOs have also been reported [164], including a measurement of ethane (C_2H_6) with a detection limit of ~1ppb in ~1 second at 3.3 μm (NNEA $= 1.2\times10^{-9}$ cm^{-1}Hz$^{-1/2}$) [91]. The theory and general aspects of WMS are well summarized in a paper by Silver [161], and discussed in more detail in papers of Axner's group [165,166].

Cavity-enhanced absorption spectroscopy

The effective absorption path length can be increased to several kilometres by coupling the mid-infrared beam into an optical cavity formed by highly reflective low-loss mirrors. High-quality dielectric mirrors with reflectivity of better than 0.9998 in the wavelength region 3-5 μm are commercially available [167]. A 1-m long cavity formed by two such mirrors leads to an optical path length of about 5 km – in other words, a photon coupled into the cavity bounces back and forth between the mirrors for 5 km on average, before escaping the cavity. This results in an enhancement of the detectable absorption by three orders of magnitude as compared to direct absorption spectroscopy, allowing trace gas detection down to the parts-per-trillion (ppt, 10^{-12}) level.

The simplest implementation of CW cavity-enhanced absorption spectroscopy (CEAS) is to measure the optical power transmitted through the cavity while scanning the wavelength of the mid-infrared OPO or DFG source. The absorption spectrum is imprinted on the transmitted power spectrum the same way as in DAS, but amplified with the enhancement factor of the cavity. This method is often referred to as integrated cavity output spectroscopy (ICOS) [168]. The light can be coupled into the cavity using the on-axis configuration (Fig. 15c), which means that the mid-infrared beam is directed to the optical cavity parallel to its optical axis. The input beam is carefully mode-matched so that only the lowest order transversal mode (TEM_{00}) of the cavity is excited. This leads to a cavity transmission spectrum that consists of peaks separated by the longitudinal mode spacing, or free spectral range $FSR = c/L_{rt}$, where L_{rt} is the round-trip length of the cavity. If the cavity length is kept constant, this means the absorption spectrum can be sampled with a frequency spacing of *FSR*, which is ~ 0.01 cm^{-1} (300 MHz) for a typical 0.5 m long standing wave cavity (L_{rt} = 1 m). This spectral resolution is sufficient in the measurements of pressure broadened mid-infrared absorption lines that have a linewidth of approximately 0.1 cm^{-1} at atmospheric pressure. An advantage of this method is that the *FSR* of the cavity is known with a relatively high accuracy, which gives a simple means to calibrate the frequency axis of the absorption spectrum. The resolution can be improved by slightly scanning the cavity length between the OPO/DFG frequency scans using a piezoelectric actuator, such that the cavity transmission spectrum moves relative to the absorption spectrum to be measured.

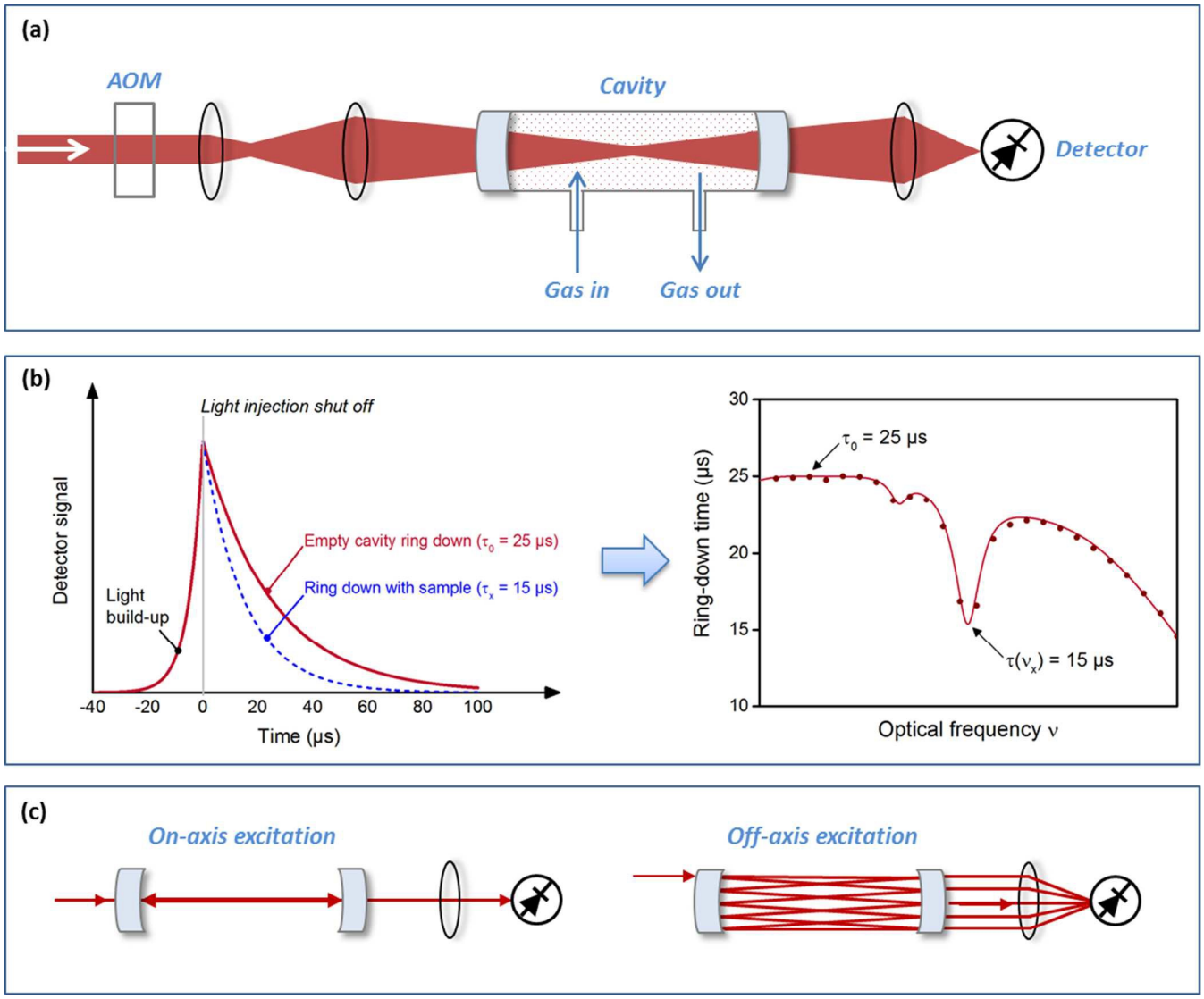

Figure 15. The principle of cavity ring-down spectroscopy. (a) The mid-infrared beam is mode matched to the cavity formed by two highly reflective mirrors. The cavity also contains the gas sample under measurement. An acousto-optic modulator (AOM) is used to switch off light injection into the cavity, so as to measure the ring down signals with a fast photo detector. (b) The light power transmitted by the cavity, as measured with the detector when the light frequency is matched with a cavity resonance frequency. The absorption spectrum of the gas sample can be deduced from the measured ring-down time vs. frequency tuning using Eq. (9). (c) Two different configurations for cavity enhanced spectroscopy: In on-axis configuration, the input beam is mode-matched to the lowest-order transversal mode (TEM_{00}) of the cavity. In re-entrant off-axis configuration, several transversal modes are excited in order to improve the spectral resolution.

The attainable trace gas detection limit of ICOS is often limited by the noise caused by fluctuations of the light and its coupling to the cavity. A common approach to mitigate this problem is to use so-called off-axis coupling (Fig. 15c), which resembles multipass alignment [169,170]. In general, a large number of high-order transversal modes are excited within one *FSR*, leading to a nearly continuous cavity transmission spectrum. Such configuration allows for fast, high-resolution spectroscopy, although the calibration of the frequency axis is lost. Another advantage is the reduction of noise caused by changes in cavity alignment and coupling [170]. Off-axis ICOS requires a relatively powerful (> 1 mW) mid-infrared light source, such as a high-power DFG source [170,169,171,172] or a CW SRO [173]. This technique has been applied to sub-ppb detection of greenhouse gases [172], as well as to breath analysis, which requires sensitive real-time monitoring of trace gases in a complex gas matrix. As an example, Arslanov *et al*. have demonstrated simultaneous detection of ethane, methane and water in exhaled breath using an off-axis ICOS spectrometer based on a CW-SRO that is tunable from 3 to 4 µm [174]. They have also reported a detection limit of 50 ppt (0.25 s) for ethane using the same setup, corresponding to an NNEA of 4.8×10^{-11} $cm^{-1}Hz^{-1/2}$ [173].

In addition to the noise arising from power fluctuations, ICOS suffers from the difficulty of accurate determination of the effective absorption path length. For this reason, the measurement needs to be calibrated separately. Both the need for calibration and the degradation of signal-to-noise ratio due

to power fluctuations can be avoided by using CW cavity ring-down spectroscopy (CRDS) [175], which is sometimes referred to as cavity leak-out spectroscopy [176]. In CRDS, light injection in the cavity is momentarily switched off using, e.g., an acousto-optic modulator, and the subsequent decay of the light field stored in the cavity is measured (Fig. 15). The decay time, or ring-down time, of the light intensity depends on the optical losses of the cavity, which gives a sensitive means to measure the absorption due to the sample gas. The absorption coefficient α at frequency ν of the light can be calculated from

$$\alpha(\nu) = \frac{1}{c}\left(\frac{1}{\tau(\nu)} - \frac{1}{\tau_0}\right) \qquad (9)$$

where τ(ν) is the ring-down time in the presence of gas that absorbs at ν. Time constant τ_0 is a reference value that indicates the decay time without any absorbing gas. Whilst often referred to as the "empty-cavity" ring-down time, τ_0 is in practice obtained by measuring the ring-down signal at a frequency where there is no absorption due to the sample gas.

In addition to being practically immune to fluctuations of the injected power, CRDS is calibration free, as the absorption coefficient can be deduced directly from the measured ring-down time (Eq. 9). Typical ring-down times with highly reflective mirrors in the 3-5 μm band are in the order of 10 μs [167]. In practice, the NNEA of a CW mid-infrared CRD-spectrometer is 10^{-8}-10^{-10} $cm^{-1}Hz^{-1/2}$, making this method very useful for the detection and analysis of small concentrations of trace gases [60,167]. As an example, von Basum *et al*. have demonstrated ppt-level detection limit for ethane in air using a CW-OPO at 3.35 μm (NNEA = 1.6×10^{-10} $cm^{-1}Hz^{-1/2}$) [176].

The most common design used in CW CRDS is based on the on-axis configuration; the off-axis configuration is rarely used, one reason being the lack of frequency-axis calibration. So-called re-entrant off-axis configuration is an exemption in this sense. By choosing the cavity length properly, it is possible to excite certain groups of degenerate cavity modes, such that the cavity transmission pattern still consists of discrete, equidistant lines, but the line spacing is an integer fraction of *FSR* [177]. Off-axis re-entrant CRDS has been applied to fast (5 ms) and sensitive (NNEA = 2.8×10^{-8} $cm^{-1}Hz^{-1/2}$) high-resolution measurements of H_2CO using a 3.4-μm CW SRO as a light source [178].

PHOTO-ACOUSTIC SPECTROSCOPY

The output power of a tunable CW OPO can be several watts, which is 1-3 orders of magnitude more than what is available from narrow-linewidth mid-infrared semiconductor lasers. The combination of high output power and broad wavelength tuning range makes the CW mid-infrared OPOs an excellent solution for trace gas detection by photo-acoustic spectroscopy (PAS) [179]. In PAS, the OPO output beam is passed through a gas sample, which is typically enclosed in a cell of a constant volume. The OPO power absorbed by the sample molecules leads to local heating of the gas, which causes a pressure increase. If the optical excitation of molecules is done periodically, for instance by chopping the power of the OPO beam, the pressure change is also periodic. This acoustic wave at the chopping frequency can be detected with a microphone, often using lock-in detection for improved signal-to-noise ratio. The voltage signal S_{PAS} measured by the microphone is

$$S_{PAS}(\nu) = C\alpha(\nu)P_0(\nu), \qquad (10)$$

where C is the instrument constant (in units V×cm/W) and $P_0(\nu)$ is the incident optical power. In other words, the detection sensitivity of PAS can be improved by increasing the power, which favours the use of high-power sources like singly-resonant OPOs.

Photo-acoustic spectroscopy is a zero-background method, because in the ideal case microphone signal is generated only when the sample molecules absorb light. In practice, some residual background signal also appears due to acoustic noise and due to absorption of the OPO light on the cell walls and windows [179]. These effects can be minimized by proper design of the experimental setup, in which case trace gas detection sensitivity comparable to that of cavity-enhanced spectroscopy can be obtained. For example, wavelength modulation can be used instead of amplitude modulation (chopping), so that a photo-acoustic signal is generated only in the presence of a frequency-dependent loss, such as an absorption line, and not due to wall absorption etc. [180,181]. A typical photo-acoustic spectrometer is intrinsically simple and compact, which makes the method suitable for field measurements. Also, the wavelength region for trace gas detection by PAS is only limited by the availability of laser sources, not by optical components. On the other hand, unlike DAS or CRDS, PAS is not an absolute method but requires calibration.

Conventional PAS instruments are based on condenser microphones or piezoelectric microphones. Up to one or two orders of magnitude improvement in detection sensitivity can be obtained by using an acoustic resonance tube, which enhances the acoustic signal [179]. The normalized noise equivalent absorption coefficient measurable with such PAS setups, when using a mid-infrared CW OPO as a light source, are typically of the order of 10^{-8}-10^{-9} $Wcm^{-1}Hz^{-1/2}$, enabling sub-ppb-level detection of ethane and other trace gases that strongly absorb between 3 and 4 μm wavelengths [50,182,183]. Note that in this case the NNEA is also normalized to optical excitation power, as the PAS sensitivity ideally improves linearly with power. The use of CW OPO-based PAS in life sciences has been demonstrated by Harren's group, one intriguing application being real-time monitoring of trace amounts of CO_2 released during the respiration of living ants [184]. The same group has also measured hydrogen cyanide (HCN) from plant leaves, from human breath, as well as from Pseudomonas bacteria [185].

Recent improvements in PAS have focussed on new innovative microphone designs, such as quartz tuning fork [186] and silicon cantilever [187] microphones. The first of

these solutions is referred to as quartz-enhanced photoacoustic spectroscopy, QEPAS, and it uses a small quartz tuning fork as a resonant acoustic transducer. Similar to more conventional approaches, an additional acoustic resonator, such as a small tube, can be used to further enhance the photoacoustic signal. Owing to the small size of a quartz tuning fork, QEPAS is suitable for the analysis of gas samples of small volume of the order of 1 mm^3. On the other hand, the small size of the resonant structure limits the effective absorption path length to a few millimetres or less, which makes detection of minuscule trace gas concentrations challenging. Nevertheless, QEPAS has been applied to ppb-level detection (NNEA = 4.4×10^{-7} $Wcm^{-1}Hz^{-1/2}$) of ethane using a widely tunable mid-infrared CW SRO [188]. Significantly better values have been reported with other lasers, such as with a quantum cascade laser at 10.5 μm [189].

Cantilever-enhanced spectroscopy (CEPAS) has also been demonstrated with a mid-infrared CW SRO. Detection limits of 190 ppt (1 s) and 65 ppt (30 s) were obtained for HCN and CH_4, respectively, corresponding to an NNEA of 1.8×10^{-9} $Wcm^{-1}Hz^{-1/2}$ [181]. In this case, the sensitivity was limited by the power and wavelength fluctuations of the OPO; an order of magnitude better NNEA can be obtained with a more stable laser [190]. The acoustic signal is detected in CEPAS by measuring the movement of the silicon cantilever with a laser interferometer. The movement of the cantilever is highly linear, and approximately two orders of magnitude larger than that of a conventional membrane microphone [187]. Together with the possibility of using relatively long gas cells (~10 cm) this makes it possible to achieve very low trace gas detection limits with CEPAS.

MID-INFRARED FREQUENCY-COMB SPECTROSCOPY

Several aspects need to be taken into account for accurate quantification of trace gas concentrations, as is discussed, for example, in Refs. [167,191]. In practice, a laser spectrometer can be calibrated using a reference gas standard, but in many cases the absorption line strengths need to be known in order to calculate the trace gas amount fractions. Absorption line strengths, as well as other line parameters like pressure broadening coefficients, of several molecular transitions are listed in spectroscopic databases, such as HITRAN [192] and GEISA [193]. Determination of the absorption line areas, which also need to be known for reliable calculation of the amount fractions, requires a calibration of the frequency/wavenumber axis of the measured absorption spectrum. This can often be accomplished with a sufficient precision by concurrently measuring the transmission spectrum of an optical etalon that has a known *FSR* [191].

Optical frequency combs have provided a new tool for accurate calibration of the frequency axis in optical spectroscopy. Frequency comb spectroscopy can be divided in two categories: Direct OFC spectroscopy, where the comb light is directly used to measure the gas spectrum, and OFC-assisted spectroscopy, where a tunable, OFC-referenced narrow-linewidth CW laser is used for spectroscopy. In OFC-assisted spectroscopy, the absolute frequency of a tunable laser can be determined during a frequency scan by a beat-frequency measurement against a fully stabilized OFC [194,195]. Alternatively, the laser frequency can be locked to the OFC, in which case the frequency scanning is carried out by tuning f_r or f_{ceo} of the comb [196].

The high cost and complexity of the mid-infrared OFCs has so far limited their spectroscopic use to laboratory conditions, and only one demonstration of the spectroscopy of outdoor air has been reported: atmospheric concentrations of CH_4 and H_2O were measured over a 26-m path with direct comb spectroscopy, using an OFC based on a synchronously pumped 3.25-μm SRO [197]. Fast acquisition times of tens of μs to 2 ms and sub-ppm detection limits were achieved using a detection scheme based on a virtual-image phased array (VIPA) etalon disperser, which is combined with a diffraction grating [6,198]. This system disperses the comb light in two dimensions, and an array camera is used to detect the 2-D picture such that that each pixel of the camera corresponds to an optical frequency. The VIPA spectrometer allows for rapid broadband measurements to be performed without the need to stabilize the OFC. The measurement resolution is typically better than 1 GHz (0.03 cm^{-1}), which is sufficient for trace gas analysis in atmospheric pressures [197]. It has been shown that the mid-infrared spectrum can be efficiently upconverted to the near-infrared region, where high-quality optical components and detectors are better available [199].

Despite the practical challenges related to the existing mid-infrared comb technology, direct OFC spectroscopy has several potential advantages over tunable laser spectroscopy in trace gas analysis. A large number of molecular transitions and species can be measured at once, often in real-time and with high sensitivity, owing to the large spectral coverage of the OFCs [200,201,202,203]. The combination of a broad spectrum and high resolution also makes it possible to better account for baseline variations and interfering spectral features due to, e.g., water absorption. This is particularly useful in applications that require detection and quantification of several trace gases simultaneously, such as in breath analysis. The same characteristics are also needed to measure complex and dense spectra of large asymmetric molecules, including many volatile organic compounds.

While the research of OFC spectroscopy has so far focused on the near-infrared region, several demonstrations in the mid-infrared region have also been reported using various methods and detection schemes, many of which are reviewed in Refs. [204,205]. The most common solution is to pass the OFC light into an external gas cell [201] or cavity [203] that contains the sample to be measured. The gas sample can also be injected inside the cavity of a mid-infrared comb generator (SP-OPO), which simultaneously serves as a multipass cell that enhances the effective absorption path length by approximately a factor of ten [206]. The mid-infrared spectrum behind the gas sample can be recorded with a low-cost optical spectrum analyser, such as a VIPA spectrometer [198] or an FTIR spectrometer [203,206]. One of the benefits of using an OFC as a light source

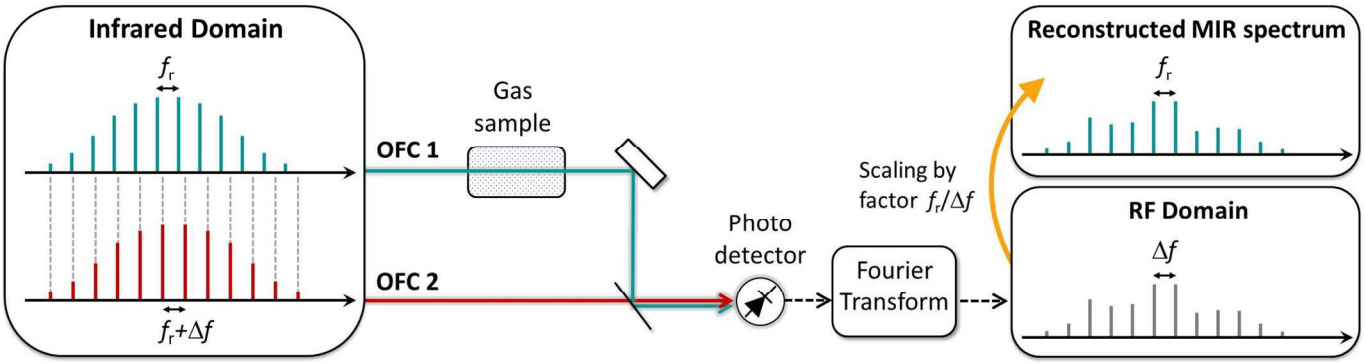

Figure 16. The basic principle of dual-comb spectroscopy. Infrared frequency comb OFC 1 is passed through the gas sample under measurement, and subsequently heterodyned with a reference frequency comb (OFC 2) at a photodetector. Owing to the slightly different repetition rates of the two combs, the heterodyne measurement produces a comb in the radiofrequency domain, such that each tooth of the RF comb unambiguously corresponds to a tooth of the infrared comb OFC 1. The infrared spectrum of OFC 1 with the gas absorption imprinted on it is obtained from the RF spectrum by multiplying the frequency axis with the scaling factor $f_r/\Delta f$.

for FTIR spectroscopy, in contrast to conventional thermal light sources, is the possibility of surpassing the interferometer-limited resolution of the FTIR spectrometer with OFCs [207].

A unique combination of fast measurement speed, good signal-to-noise ratio, high spectral resolution, and excellent frequency accuracy can be obtained using dual-comb spectroscopy, which resembles the FTIR method but does not require any moving parts [201,202,208,209]. The generation of an FTIR-type interferogram can be understood by considering the dual-comb method as a form of optical time-domain spectroscopy: The beam from one of the combs passes the gas sample while the other comb is used as a reference. The beams of these two combs are superimposed on a photodetector. Owing to slightly different pulse repetition rates of the two combs, the timing between the pulses varies over time, making it possible to construct the electric field of the measuring pulse as a function of time. Fourier transform of this time-domain signal (interferogram) gives the spectrum. The dual-comb method can also be viewed as a multiheterodyne measurement, which converts the optical spectrum to the radiofrequency regime, where it can be easily recorded in real time (Fig. 16) [208]. This method is somewhat demanding to implement, because it in general requires two stabilized combs. This requirement is often easier to meet in the near-infrared region, especially because the two combs can be phase-coherently generated from a single laser [210,211,212,213]. Moreover, successful dual-comb measurements with mutually non-stabilized OFCs have been reported in the near-infrared region [214].

In addition to actual trace gas detection, accurate OFC spectroscopy is also useful for gathering improved data for spectroscopic databases that form an essential tool for real-world applications – after all, the accuracy of trace gas spectroscopy often depends on the quality of these databases [167]. As an example, Baumann *et al*. have used dual-comb spectroscopy to measure 132 rovibrational lines of the *P*, *Q*, and *R* branches of the ν_3 band of CH_4 at ~3.4 μm [201]. Their estimated systematic uncertainty in the determination of line centre frequencies was 300 kHz, which is an order of magnitude improvement compared to prior data collected using conventional FTIR spectroscopy. The uncertainty mainly arises from the spectroscopic shifts, since the frequencies of the mid-infrared comb lines were known with an accuracy of better than 100 Hz.

The need for accurate, high-resolution measurements for the improvement of molecular databases has motivated several groups to investigate OFC-assisted mid-infrared spectroscopy [37,59,81,195,215,216,217]. The schemes developed so far can be divided in two categories: The comb can be used as a ruler to calibrate the frequency axis during CW laser frequency scans [195], or the CW laser frequency can be locked to the OFC, typically such that there is a small frequency offset ($< f_r$) between the laser and the nearest comb tooth [217]. With tight phase locking between the laser and the comb, via either electronic feedback or optical injection locking [218], the accuracy of the mid-infrared frequency is ultimately limited by the uncertainty of the microwave frequency standard used as a reference for the OFC [196]. The frequency of the mid-infrared laser can be scanned with a high precision by changing this lock offset, although a small discontinuity is often inevitable at frequencies where the lock offset, i.e., the beat frequency between the laser and the comb, is zero or $f_r/2$. These discontinuities can be avoided by using another scanning method, where the lock offset is kept constant while the comb repetition frequency is scanned [46,80]: According to Eq. (7), the change in the mid-infrared frequency of a comb tooth is equal to the change of f_r multiplied by m, which is the mode number of the tooth. The mid-infrared frequency can also be swept by changing the comb offset frequency, but in most OFCs the offset tuning range is small, of the order of f_r.

The most important configurations for OFC-assisted mid-infrared spectroscopy are illustrated in Fig. 17. One of the approaches is to use a parametrically generated mid-infrared frequency comb to which a CW mid-infrared source is referenced (Fig. 17a) [171,219]. However, as the generation of fully-stabilized high-power OFCs in the mid-infrared region is challenging, a more common approach relies on the use of a CW mid-infrared source that is derived from near-infrared

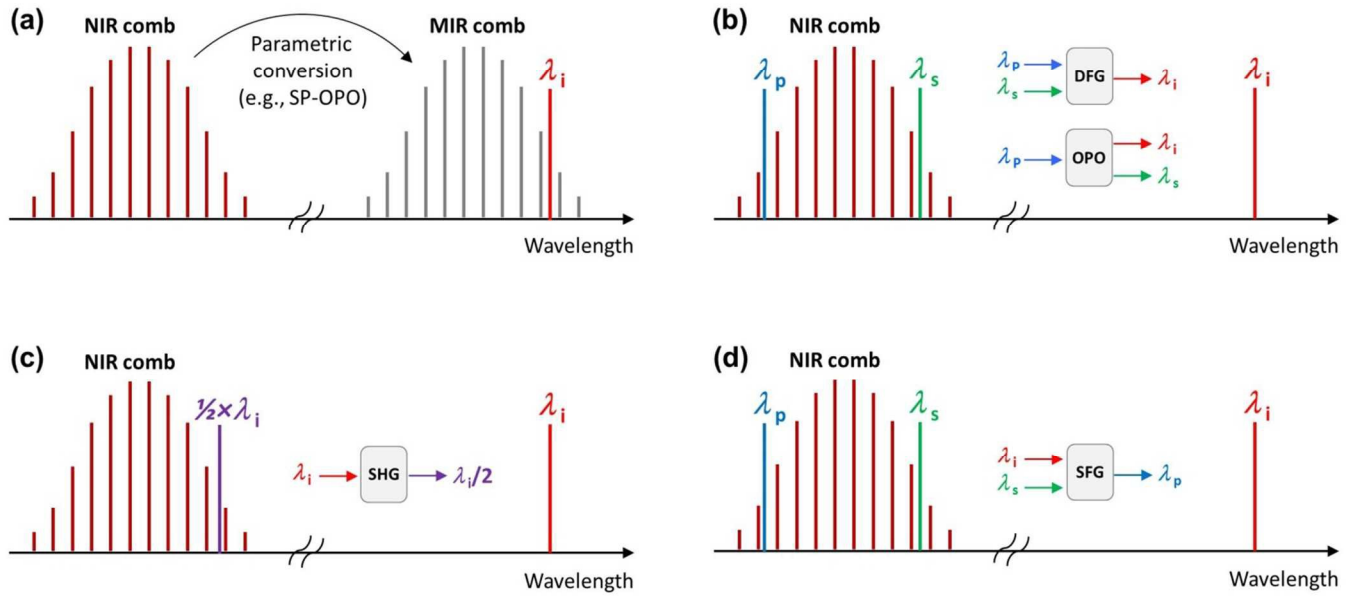

Figure 17. Four different schemes for referencing an infrared wavelength λ_i to an optical frequency comb. (a) Direct beat-frequency measurement with a parametrically generated mid-infrared frequency comb, (b) referencing of pump and signal wavelengths of a CW DFG or OPO source to a near-infrared frequency comb, (c) referencing the mid-infrared wavelength to a near-infrared frequency comb after second harmonic generation (SHG), and (d) after sum-frequency generation (SFG).

lasers by parametric generation; a continuous-wave OPO or DFG source can be directly referenced to a fully stabilized near-infrared OFC (Fig. 17b). For instance, the standard mid-infrared DFG is based on 1064-nm and 1550-nm lasers, which can both be directly locked to an OFC produced by an Er-doped mode-locked fibre laser [196,215,216]. The same approach also works with a CW OPO [59,79,81,82]. An advantage of this method is that as both the pump and signal frequencies are referenced to the same comb, the comb offset frequency f_{ceo} cancels out and does not need to be stabilized or known [216]. On the other hand, it is difficult to perform large frequency scans by tuning the repetition frequency of the OFC if ν_p and ν_s are both locked to it. A wide continuous sweep of the mid-infrared frequency requires that these both frequencies can be scanned without mode hops over large ranges, which becomes an issue especially with CW OPOs. Use of an external frequency tuning apparatus, such as an electro-optic modulator (EOM), provides a potential cure to this problem. Although the typical tuning range attained by an EOM is limited to a few hundred MHz or less [78], scanning ranges of tens of GHz are potentially possible with modern EOMs or with an innovative new method called "endless frequency scanning", which is not limited by the tuning range of the EOM [220,221].

Another solution that avoids the problem of limited scanning range is to directly link the mid-infrared frequency to a near-infrared OFC. This can be done by second harmonic generation (frequency doubling) [83] or by sum-frequency generation [217], as illustrated in Figs. 17c and 17d, respectively. Second harmonic generation works particularly well with CW SROs that have high enough output power for efficient single-pass frequency doubling in a nonlinear crystal [83]. In practice, any output wavelength of the CW SRO between 2 and 4 μm can be locked to the Er-fibre OFC, which spans from 1 to 2 μm. The repetition frequency of a typical Er-fibre OFC can be tuned by approximately 1%, which corresponds to a continuous tuning over several hundred GHz of the mid-infrared beam locked to the comb.

Comb-assisted spectroscopy in the mid-infrared region has been used to measure molecular absorption line parameters with high accuracy; especially the ν_3 band of CH_4 centred at 3.4 μm has been extensively studied [201,216,222,223,224]. The high optical power and narrow linewidth makes the CW mid-infrared sources ideal for saturated absorption spectroscopy either in dual-pass or cavity enhanced geometry. The resulting sub-Doppler resolution is particularly useful for the precise determination of line centre frequencies, as has been demonstrated, e.g., by the group of Sasada. They have used a narrow-linewidth DFG source and cavity-enhanced wavelength modulation spectroscopy to measure the centre frequencies of more than 200 absorption lines of the CH_4 ν_3 band at ~3.2 to 3.5 μm [222,223]. The same group has also published accurate centre frequencies of several hyperfine components of the fundamental vibration bands of two isotopomers of hydrogen chloride, $H^{35}Cl$ and $H^{37}Cl$, at ~2900 cm^{-1} [225].

Parametric CW sources referenced to OFCs are useful for the purposes of frequency metrology in general, for example to perform direct phase-coherent comparisons of mid-infrared and near-infrared frequency standards (molecular clocks), as has been demonstrated by Kovalchuk *et al*. [79]. It is also expected that the excellent frequency precision provided by tunable OFC-locked lasers open new opportunities in applications that require uttermost trace gas detection sensitivity. As an example,

Galli *et al*. have reported parts-per-quadrillion (ppq, 10^{-15}) level detection of radiocarbon-dioxide ($^{14}CO_2$) with OFC-assisted CRDS at 4.5 μm wavelength [226]. The exceptionally high detection sensitivity was largely due to the long acquisition time of 1 h, which was made possible by the good frequency accuracy of the OFC-locked DFG source used in the experiments.

3.2. Basic research

The use of mid-infrared frequency combs and CW OPOs in the field applications of trace gas analysis is still marginal because of the limited commercial availability and relatively high cost and complexity of these instruments. Several applications of parametrically generated mid-infrared light sources in fundamental research, on the other hand, have been reported during the past few years. In the following, we briefly review some of these applications, many of which rely on high-resolution rovibrational spectroscopy in the C-H stretching region, close to the 3 μm wavelength. We also introduce the basics and recent developments of the mid-infrared laser spectroscopy methods that are most relevant for the research areas discussed here.

NEUTRAL MOLECULES

Both CW OPOs and DFG sources have been used to study the vibrational bands of several molecules in the mid-infrared region. Many of these studies have been made in conditions relevant to atmospheric chemistry or environmental monitoring, therefore falling in the same category as the already discussed work on the improvement of spectroscopic databases. From the fundamental research point of view, it is worth pointing out that accurate studies of molecular absorption lines are also valuable for tests of quantum mechanics theories [227], as well as for the determination of molecular constants [225]. As an example, a detailed analysis of the ν_3 fundamental vibrational mode of gas-phase Si_2C_3, as well as of the $(\nu_3+\nu_7)-\nu_7$ hot band, has been carried out based on recent high-resolution measurements with a CW SRO at 5 μm [86,228].

Another good example of a fundamentally oriented research is a work of our group, where a novel spectroscopy method was developed to study such vibrational states that are not directly accessible from the vibrational ground state by one-photon transitions. This so-called infrared stimulated emission probing (IRSEP) method was demonstrated by measuring symmetric rovibrational states of acetylene (C_2H_2) [229]. The molecules were first pumped from the vibrational ground state to an asymmetric state using a near-infrared laser, after which stimulated emission was detected using a tunable mid-infrared CW SRO as a probe. This method provides a sub-Doppler resolution and a high signal-to-noise ratio that is an order of magnitude better compared to a previous technique where spontaneous fluorescence was detected instead of stimulated fluorescence. The IRSEP method has provided new spectroscopic data and molecular parameters of the vibrational state $3\nu_1$ of C_2H_2, which was observed for the first time [229]. Further improvements are expected with another new two-photon method which combines intense CW SRO pumping with near-infrared CRDS. In this method, the acetylene molecules are first pumped to an asymmetric vibrational intermediate state by the SRO, and the transition to a symmetric state (of a higher energy) is subsequently probed by CRDS. The method has already been demonstrated by measuring the $\nu_1 + 2\nu_3$ state of acetylene [230].

Spectroscopy of complex molecules and molecular complexes is challenging in atmospheric conditions owing to their broad absorption spectra that consist of a vast number of closely spaced lines [231]. One of the most popular methods for high-resolution studies of such molecules is to inject the gas into the detection region by supersonic jet expansion, which is typically oriented perpendicular to the laser beam used for spectroscopy, as illustrated in Fig. 18. This arrangement enables effective translational, rotational, and even vibrational cooling, which simplifies the absorption spectra and permits their measurements with sub-Doppler resolution [232]. An additional advantage of using molecular beams formed by supersonic expansion is the possibility of efficient preparation of the molecules in a specific rovibrationally excited state by either chemical reactions [233,234] or infrared laser pumping [235]. The jet expansion method is convenient to combine with direct absorption spectroscopy and multipass cells [233], but can also be implemented within a ring-down cavity [231].

The jet expansion method is particularly useful for the measurements of molecules that have dense absorption spectra [231]. As an example, the C−H antisymmetric stretching mode ν_4 of diacetylene (HC_4H) and the associated hot bands around 3333 cm^{-1} have recently been studied by Chang and Nesbitt using slit-jet cooling [233]. Their spectrometer was based on a tunable CW DFG source and a Herriot-type multipass cell, which was placed along the long axis of the slit jet expansion. Diacetylene was generated in situ starting from discharge dissociation of acetylene in the pulsed supersonic slit expansion. The diacetylene concentration was modulated with the discharge so as to improve the measurement sensitivity by

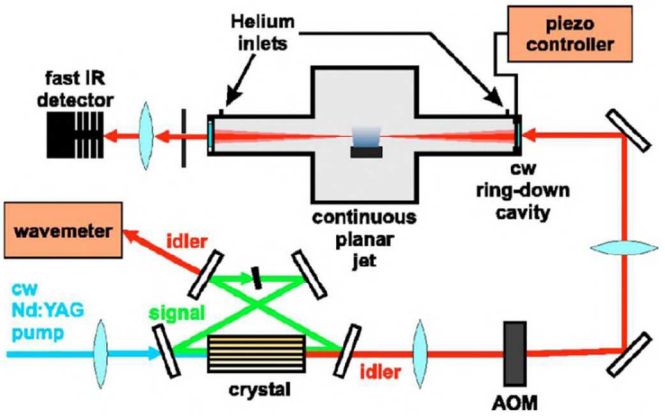

Figure 18. Use of a CW SRO for mid-infrared CRDS of complex molecules in supersonic planar jet expansion, which is placed inside of the ring-down cavity. The helium flow at both ends of the cavity is used to protect the highly reflective cavity mirrors from contamination. Reproduced with permission from [231].

lock-in detection of the modulated absorbance signal. Sub-Doppler resolution of the experiment permitted observations of both rotational structure and Coriolis interactions in the ν_4 stretch.

Linnartz's group has successfully implemented the jet expansion inside a high-finesse optical cavity, in order to improve the sensitivity of the absorption measurements using CRDS. As a light source they use a widely tunable mid-infrared CW SRO in the 3 μm region. This combination has permitted high-resolution studies of several molecular species that are of interest in astrochemistry, including HC_4H [234], HC_6H [236,237], and propyne [238]. Also here, the carbon-chain species HC_4H and HC_6H were produced in situ using a slit-jet discharge nozzle. The detection sensitivity of a typical jet-expansion CRDS setup is of the order of 10^{-7} $cm^{-1}Hz^{-1/2}$ [231,236]. This is one to two orders of magnitude worse than that is usually obtained by mid-infrared CRDS of static gas samples, mainly owing to the limited absorption path length through the expansion and the lower effective geometrical coverage of the mid-infrared beam in the expansion [231]. On the other hand, the spectroscopic selectivity is greatly enhanced compared to the measurement of room-temperature gas samples.

The detection sensitivity can be further improved by using a technique called noise-immune cavity-enhanced optical heterodyne molecular spectroscopy (NICE-OHMS). NICE-OHMS is an ultrasensitive variant of FMS, and is capable of providing an NNEA as good as 10^{-14} $cm^{-1}Hz^{-1/2}$ in the near-infrared region [239]. This significantly exceeds the sensitivity of even the most sophisticated CRD-spectrometers based on laser locking, which share the same level of complexity [240,241,242,243]. As the name implies, the NICE-OHMS method combines cavity-enhanced spectroscopy with frequency modulation (heterodyne) spectroscopy. The details of the method are discussed, e.g., in Refs. [239,244]. In brief, the centre frequency of the laser used for FMS is tightly locked to a cavity resonance using the Pound-Drever-Hall technique [245,246]. The high sensitivity is then achieved by choosing the modulation frequency of FMS such that it exactly matches the *FSR* of the cavity. This selection makes the system essentially immune to laser frequency noise, as it avoids the conversion of frequency noise into amplitude noise by the cavity.

The use of NICE-OHMS spectroscopy in the mid-infrared region was first demonstrated with a quantum cascade laser [247], and later with parametric sources [248,249]. While the required high-speed frequency modulation of a mid-infrared beam is difficult to do externally, the modulation can be carried out via the near-infrared pump beam of a CW DFG source or a CW SRO. Detection sensitivities of the order of 10^{-9} $cm^{-1}Hz^{-1/2}$ have been reported for the NICE-OHMS spectroscopy of CH_4 using such an approach [248,249]. This level of performance is still far from the shot-noise limit, but further improvements are expected [249]. Despite the potentially high performance, mid-infrared NICE-OHMS spectroscopy has not yet gained significant interest in the spectroscopy of neutral molecules. The research of charged molecules, on the other hand, has already greatly benefitted from this method, as discussed in the following.

MOLECULAR IONS

Spectroscopy of molecular ions is an example of a research area where mid-infrared CW SROs have been actively used during the past few years. The first mid-infrared CW SRO experiment in this field was reported in 2007, when a rotationally resolved spectrum of the ν_1-stretch of the astrophysically relevant HCO^+ at 3.2 μm was measured by Linnartz's group [250]. The experimental arrangement was essentially the same as that discussed above in the context of neutral molecules research: The authors combined a widely tunable CW SRO with CRDS, and obtained sub-Doppler resolution by translational and rotational cooling of the ions using supersonic plasma expansion inside the ring-down cavity.

High-resolution CW SRO spectroscopy of the ν_1 band of HCO^+ has also been reported by the group of McCall [251]. They have developed a new technique called noise-immune cavity-enhanced optical heterodyne velocity modulation spectroscopy (NICE-OHVMS) [252]. The NICE-OHVMS method combines two state-of-the-art spectroscopy techniques, NICE-OHMS and velocity modulation spectroscopy. This combination provides a sub-Doppler resolution and an impressive sensitivity of $\sim 10^{-9}$ $cm^{-1}Hz^{-1/2}$ in the mid-infrared spectroscopy of molecular ions, such as H_3^+ [253,254], HCO^+ [254], and CH_5^+ [254]. A high frequency accuracy can be obtained by referencing the mid-infrared idler beam of the CW-SRO used for spectroscopy to a stabilized near-infrared OFC [251]. The key to selective detection of molecular ions is velocity modulation spectroscopy, which was originally developed by Saykally's group in 1980's [255]. This method is typically used with a CW laser, although massively parallel detection with a near-infrared OFC has also been demonstrated [256]. Velocity modulation spectroscopy is based on the modulation of plasma velocity by modulating the polarity of a gas discharge. This leads to a modulation of the respective Doppler shift, allowing one to discriminate the absorption due to the charged species against that of the neutral species, which in most cases are several orders of more abundant and would otherwise obscure the weak absorption signal of the ions.

Methods for OFC-calibrated CW-SRO spectroscopy of molecular ions in the mid-infrared wavelengths have also been developed by Schlemmer's group. In particular, they have applied a mid-infrared CW SRO to mass-selective action spectroscopy based on light induced reactions (LIR), in order to study trapped molecular ions in cryogenic temperatures. The focus of these studies has been on molecular ions that are of importance in astrochemistry, such as CH_2D^+ [257], *l*–C_3H^+ [258], and CH_5^+ [259]. They have also demonstrated a new two-photon LIR scheme for direct rotational spectroscopy of trapped ions [257,260]. In this scheme, a CW-SRO is used to pump a rovibrational transition starting from a rotational level of the vibrational ground state, leading to a constant LIR signal. Terahertz radiation then excites a pure rotational transition within the vibrational ground state, thus decreasing or increasing the LIR signal stemming from the mid-infrared

excitation. This method can be applied to pure rotational spectroscopy of, e.g., deprotonated water OH^-, for which one-photon terahertz excitation does not work [260].

NANODROPLET AND MATRIX ISOLATION SPECTROSCOPIES

In addition to supersonic jet expansions, matrix isolation and helium nanodroplet isolation (HENDI) [261] offer a possibility to study molecules in low-temperature environments. The first photochemical use of a mid-infrared CW SRO in a matrix-isolation experiment was reported by Marushkevich *et al*. in 2009 [262]. They used a high-power CW SRO to promote conformational changes of matrix-isolated formic acid by selective vibrational excitation at ~3500 cm^{-1}. By combining this mid-infrared excitation with thermal annealing of the matrix, the authors evidenced formation of five new dimers of formic acid in an argon matrix.

A large number of high-resolution spectroscopy studies of various molecules captured in superfluid ^{4}He nanodroplets have been performed during the past few years using tunable CW SROs, especially by the group of Douberly. In their typical HENDI experiment, the helium droplets are generated by expanding helium gas through a cryogenically cooled nozzle. The droplets are subsequently cooled to ~0.4 K via evaporation, and skimmed into a collimated droplet beam [261]. The mean size of the droplets is typically a few thousand atoms. The droplet beam is passed through a measurement cell prior to entering a quadrupole mass spectrometer that is used to analyse the droplets. The cell consists of two parallel gold-coated mirrors to which a static electric field can be applied for Stark spectroscopy. These mirrors also compose a multipass cell for a mid-infrared beam from an automated high-power (> 1W) CW SRO [85], which is used to vibrationally excite the molecules embedded in the droplets. Upon vibrational excitation, the energy deposited into the embedded molecules is quenched by evaporation of helium atoms from the droplet. This shrinkage of the droplet reduces their ionization cross section, which is observed as a decrease in the signal of the mass spectrometer.

Helium nanodroplet spectroscopy is often used to study radicals and weakly bound complexes [261]. As an example, Douberly´s group has applied their OPO-based setup to measure the inertial dipole moment components of the hydridotrioxygen radical (*trans*-HOOO), in order to shed light on the question of the abundance of HOOO in the atmosphere and its role as a sink for hydroxyl radicals [263]. Together with the group of Vilesov, they have also conducted a lot of work on molecular complexes [264,265,266,267]. For instance, they assembled small $(HCl)_m(H_2O)_n$ clusters in helium nanodroplets, and measured the cluster spectra in the HCl stretch region. Using a CW SRO for high-resolution scans, the authors assigned sharp bands in this region to specific cluster compositions and structures [264,268]. A HENDI setup essentially similar to that use by Douberly's group has also been used by the group of Havenith. They have investigated allyl radical in particular, as well as its reactions and complexation in nanodroplets [269,270,271]

COLD ATOMS AND MOLECULES

In the aforementioned research of trapped molecular ions, the cooling of the sample is achieved by exposing the ions to cryogenically cooled helium atoms. This method is suitable for studies in astrochemistry, as it permits cooling down to ~4 K, which is close to the lowest temperature (~3 K) in interstellar space. Similar temperatures can be reached in cryogenically cooled matrixes and ^{4}He nanodroplets – although further cooling of the droplets down to ~0.4 K is typically achieved by evaporation. The supersonic jet expansion method, on the other hand, produces a flow of isolated gas molecules, with a narrow velocity distribution that is kinetically "cold" albeit the maximum of the velocity distribution shifts to a high value [232]. A very different type of cooling method is laser cooling, which makes it possible to create ultracold gases of atoms or molecules. As an example, KBr molecules in their absolute ground state (lowest electronic, vibrational, rotational, and hyperfine energy state) with a translational temperature of a few hundred nanokelvins have been created starting from laser-cooled atoms [272,273].

Most of the work done so far on cold atoms and molecules is based on the use of visible and near-infrared lasers, although the use of a narrow mid-infrared transition of a laser-cooled single barium ion for metrology purposes has been proposed [274]. The only laser-cooling experiments where parametric mid-infrared sources have been applied, as far as we are aware of, are those reported by Killian's group. In 2009, they published one of the first demonstrations of Bose-Einstein condensation of ^{84}Sr [275]. As usual for alkaline earth metals (as well as for alkaline metals, which are more commonly used in laser-cooling experiments), the actual transitions for cooling and trapping for strontium are in the visible or near-infrared region. A tunable mid-infrared source can, however, be useful for repumping, i.e., to return the atoms back to the laser cooling cycle in case they decay to "dark" states. As an example, efficient repumping of all stable isotopes of strontium, ^{84}Sr, ^{86}Sr, ^{87}Sr, and ^{88}Sr, has been demonstrated with a 3-µm CW SRO. Laser-cooled strontium atoms prepared with this repumping scheme have been used to study ultracold atomic collisional properties [276]. They also offer a basis to investigate cold molecules. As an example, one of the possible ways of creating cold (< 1 K) or ultracold (< mK) diatomic molecules is photo association spectroscopy, in which two colliding atoms absorb a laser photon to form an excited molecule. Coupling to a ground-state molecule can be attained by an additional laser. Starting from laser-cooled strontium atoms trapped in an optical dipole trap, Killian's group has used the two-photon photo association technique to determine the energies of selected vibrational bound states of both $^{86}Sr_2$ and $^{88}Sr_2$ dimers [277].

It is likely that in the future the coherent parametric sources suitable for high-resolution spectroscopy will find a number of new applications in the research of cold molecules, owing to the fundamental vibrational spectra of many molecular species in the mid-infrared region. One of the exciting new possibilities is the precise control of chemical reactions in ultracold gases by

infrared excitation [278]. Also, it has been proposed that high-power mid-infrared lasers tuned to vibrational resonances could be used to decelerate and trap molecules via the dipole force [279].

Molecules on Surfaces

One of the latest applications for mid-infrared CW OPOs is the chemistry at gas-surface interfaces [280]. Beck's group has studied CH_4 and H_2O on nickel surfaces, a system that is important in steam reforming of natural gas (CH_4) to produce H_2 [281,282]. In the reported experiments, the methane was applied on the Ni(100) surface in a supersonic molecular beam [282]. A high-power mid-infrared CW SRO was used for state preparation and alignment, so as to produce vibrationally excited CH_4 molecules for the investigation of alignment-dependent reactions on the surface. Similar experimental arrangement has also been used to study the physisorption of CH_4 on a Pt(111) surface, as well as to measure the sticking probability of heavy water (D_2O) on ice surfaces [283]. In Ref. [284], double-resonance excitation with two mid-infrared CW SROs was applied to measure CH_4 chemisorption on a cold Pt(111) surface. The double-resonance scheme was used to prepare the CH_4 molecules into all three vibrational symmetry components of the $2\nu_3$ antisymmetric stretch overtone vibration [235], making it possible to investigate the role of vibrational symmetry on the vibrational activation of the dissociative chemisorption [282,284].

Summary and outlook

Tunable continuous-wave DFG sources for high-resolution mid-infrared spectroscopy have been available since 1990's. The recent development of new lasers and nonlinear optical components, such as high-quality PPLN waveguide crystals, has made it possible to reach milliwatt level mid-infrared powers with relatively inexpensive and compact DFG systems that are suitable for field applications [45]. Both the output power and wavelength tuning range can be further improved by using a singly resonant CW OPO instead of a difference frequency generator. Watt-level single-mode output power and tuning ranges of hundreds of nanometres make the CW SROs well suited for, e.g., photoacoustic spectroscopy of hydrocarbons and other trace gas molecules [181].

Widespread use of CW SROs in field applications has so far been prohibited by the relatively high cost and complexity of these instruments. In the laboratory, normalized noise-equivalent absorptions as small as 10^{-9}-10^{-11} $cm^{-1}Hz^{-1/2}$ have been achieved using both CW OPOs and DFG sources in combination with state-of-the-art absorption spectroscopy methods, such as cavity-enhanced spectroscopy and photoacoustic spectroscopy. This corresponds to parts-per-billion to parts-per-trillion level detection limits in real-time measurements of typical trace gas molecules that have strong fundamental vibrational transitions within the atmospheric window, between 3 and 5 μm. Even better sensitivity can be achieved by using long acquisition times. As an example, parts-per-quadrillion level measurements of $^{14}CO_2$ have been demonstrated at 4.5 μm by using an averaging time of 1 h [226]. Such a long averaging time was made possible by phase locking the mid-infrared source to an optical frequency comb. In general, OFC-assisted spectroscopy has become an important tool for applications that require uttermost measurement precision and sensitivity.

Direct OFC spectroscopy can lead to unpresented accuracy and sensitivity in simultaneous detection of several molecular species, as has already been demonstrated in many laboratory experiments both in the near-infrared and mid-infrared regions [205]. With the foreseen progress towards compact mid-infrared comb generators, direct OFC spectroscopy is expected to stimulate advances in the field applications of molecular spectroscopy, in particular in applications that require real-time analysis of complex gas matrixes, such as exhaled breath. Even faster temporal resolution is needed in reaction kinetics, where OFC-based sensitive multispecies detection in the microsecond timescale has already proven useful [285]. On the other hand, high-power femtosecond pulses produced by broadband mid-infrared OFC generators also have significant potential in state-of-the-art laboratory experiments, for instance in the field of high-harmonic generation and ultrafast optics [101,286]. Another rapidly evolving field of science that is likely to benefit from the recent developments of coherent mid-infrared sources is the research of cold molecules. Tunable, narrow-linewidth light from CW OPOs can potentially be used to cool, trap and control molecules using the strong fundamental vibrational transitions.

Acknowledgements

University of Helsinki and the Academy of Finland are acknowledged for financial support.

Notes and references

[a] Laboratory of Physical Chemistry, Department of Chemistry, P.O. Box 55 (A.I. Virtasen aukio 1), FI-00014 University of Helsinki, Finland. E-mail: markku.vainio@helsinki.fi, lauri.halonen@helsinki.fi. Web page: http://www.helsinki.fi/kemia/fysikaalinen/research/molspec/index.html

[b] VTT Technical Research Centre of Finland Ltd., Centre of Metrology MIKES, P.O. Box 1000, FI-02044 VTT, Finland.

1 J. Hodgkinson and R. P. Tatam, *Meas. Sci. Technol*., 2013, **24**, 012004.

2 O. Vaittinen, F. Schmidt, M. Metsälä and L. Halonen, Current Analytical Chemistry, 2013, **9**, 463-475.

3 J. Kauppinen and J. Partanen, *Fourier Transforms in Spectroscopy*, Wiley, 2011.

4 D. J. Jones, S. A. Diddams, J. K. Ranka, A. Stenz, R. S. Windeler, J. L. Hall and S. T. Cundiff, *Science*, 2000, **288**, 635-639.

5 T. Udem, R. Holzwarth and T. W. Hansch,, *Nature*, 2002, **416**, 233–237.

6 S. A. Diddams, L. Hollberg and V. Mbele, Nature, 2007, **445**, 627-630.

7 I. Coddington, W. C. Swann and N. R. Newbury, *Phys. Rev. Lett*., 2008, **100**, 013902.

8 Y. Yao, A. J. Hoffman and C. F. Gmachl, *Nature Photonics*, 2012, **6**, 432-439.

9 L. E. Myers, R. C. Eckardt, M. M. Fejer, R. L. Byer, W. R. Bosenberg and J. W. Pierce, *J. Opt. Soc. Am. B*, 1995, **12**, 2102-2116.
10 D. N. Nikogosyan, *Nonlinear Optical Crystals: A Complete Survey*, Springer US, 2005.
11 P. E. Powers, *Fundamentals of Nonlinear Optics*, CRC Press, 2011.
12 E. A. Bahaa and M. C. Teich, *Fundamentals of Photonics*, 2nd Edition, Ch. 21, Wiley, 2007.
13 G.D. Boyd and D.A. Kleinman, *J. Appl. Phys*., 1968, **39**, 3597-3639.
14 P. Canarelli, Z. Benko, R. Curl and F. K. Tittel, *J. Opt. Soc. Am. B*, 1992, **9**, 197-202.
15 P. Maddaloni, G. Gagliardi, P. Malara and P. De Natale, *Appl. Phys. B*, 2005, **80**, 141-145.
16 W. Chen, J. Cousin, E. Poullet, J. Burie, D. Boucher, X. Gao, M. W. Sigrist and F. K. Tittel, *Comptes Rendus Physique*, 2007, **8**, 1129-1150.
17 J.-J. Zondy, *Opt. Commun*., 1998, **149**, 181-206.
18 T. Andres, P. Haag, S. Zelt, J.-P. Meyn, A. Borsutzky, R. Beigang and R. Wallenstein, *Appl. Phys. B*, 2003, **76**, 241-244.
19 H. Ishizuki and T. Taira, *Opt. Express*, 2008, **16**, 16963-16970.
20 G. Hansson, H. Karlsson, S. Wang and F. Laurell, *App. Opt*., 2000, **39**, 5058-5069.
21 J. R. Schwesyg, M. Falk, C. R. Phillips, D. H. Jundt, K. Buse and M. M. Fejer, *J. Opt. Soc. Am. B*, 2011, **28**, 1973–1987.
22 G. L. Tangonan, M. K. Barnoski, J. F. Lotspeich and A. Lee, *Appl. Phys. Lett*, 1977, **30**, 238-239.
23 H. Ishizuki and T. Taira, *Opt. Express*, 2010, **18**, 253-258.
24 G. K. Samanta, G. R. Fayaz, Z. Sun and M. Ebrahim-Zadeh, *Opt. Lett*., 2007, **32**, 400-402.
25 S. Zaske, D.-H. Lee and C. Becher, *Appl. Phys. B*, 2010, **98**, 729-735.
26 K. L. Vodopyanov, O. Levi, P. S. Kuo, T. J. Pinguet, J. S. Harris, M. M. Fejer, B. Gerard, L. Becouarn and E. Lallier, *Opt. Lett.*, 2004, **29**, 1912-1914.
27 V. Petrov, *Progress in Quantum Electronics*, 2015, **42**, 1-106.
28 P. D. Mason and L. F. Michaille, *Proc. of SPIE*, 2008, **7115**, 71150N-1- 71150N-10.
29 A.V. Smith, SNLO software, ver. 65 (June 11, 2015), available at http://www.as-photonics.com/snlo.
30 D. H. Jundt, *Opt. Lett.,* 1997, **22**, 1553-1555.
31 O. Gayer, Z. Sacks, E. Galun and A. Arie, *Appl. Phys. B*, **208**, 91, 343-348.
32 O. Paul, A. Quosig, T. Bauer, M. Nittmann, J. Bartschke, G. Anstett and J.A. L'huillier, *Appl. Phys. B*, 2007, **86**, 111-115.
33 C.R. Phillips, C. Langrock, D. Chang, Y. W. Lin, L. Gallmann and M. M. Fejer, *J. Opt. Soc. Am. B*, 2013, **30**, 1551-1568.
34 T. Umeki, M. Asobe, Y. Nishida, O. Tadanaga, K. Magari, T. Yanagawa and H. Suzuki, *Opt.Lett*., 2007, **32**, 1129–1131.
35 D. Richter, A. Fried, B.P. Wert, J.G. Walega and F.K. Tittel, *Appl. Phys. B*, 2002, **75**, 281-288.
36 L. Goldberg, W. K. Burns and R. W. McElhanon, *Opt. Lett*., 1995, **20**, 1280-1282.
37 C.-C. Liao, Y.-H. Lien, K.-Y. Wu, Y.-R. Lin and J.-T. Shy, *Opt. Express*, 2013, **21**, 9238-9246.
38 K. P. Petrov, W. Waltman, U. Simon, R. F. Curl, F. K. Tittel, E. J. Dlugokensky and L. Hollberg, *Appl. Phys. B*, 1995, **61**, 553-558.
39 M. F. Witinski, J. B. Paul and J. G. Anderson, *Appl. Opt*., 2009, **48**, 2600-2606.
40 I. Galli, S. Bartalini, S. Borri, P. Cancio, G. Giusfredi, D. Mazzotti and P. De Natale, *Opt. Lett.*, 2010, **35**, 3616-3618.
41 M. Lukowski, C. Hessenius, R. Bedford and M. Fallahi, *Opt. Lett*., 2015, **40**, 4174-4177.
42 E. J. Lim, H. M. Hertz, M. L. Bortz and M. M. Fejer, *Appl. Phys. Lett*., 1991, **59**, 2207-2209.
43 K. P. Petrov, A. T. Ryan, T. L. Patterson, L. Huang, S. J. Field and D. J. Bamford, *Appl. Phys. B*, 1998, **67**, 357-361.
44 D. Hofmann, G. Schreiber, C. Haase, H. Herrmann, W. Grundkötter, R. Ricken and W. Sohler, *Opt. Lett*. 1999, **24**, 896-898.
45 M. Asobe, O. Tadanaga, T. Yanagawa, T. Umeki, Y. Nishida and H. Suzuki, *Electron. Lett.*, 2008, **44**, 288–289.
46 K. Iwakuni, S. Okubo and H. Sasada, *Opt. Express*, 2013, **21**, 14832-14840.
47 A. Henderson and R. Stafford, *Opt. Express*, 2006, **14**, 767–772.
48 I. Breunig, D. Haertle and K. Buse, *Appl. Phys. B,* 2011, **105**, 99-111.
49 A. J. Henderson, P. M. Roper, L. A. Borscowa and R. D. Mead, *Opt. Lett*., 2000, **25**, 1264-1266.
50 F. Müller, A. Popp, F. Kühnemann and S. Schiller, *Opt. Express*, 2003, **11**, 2820-2825.
51 W. R. Bosenberg, A. Drobshoff, J. I. Alexander, L. E. Myers and R. L. Byer, *Opt. Lett*., 1996, **21**, 1336-1338.
52 M. Vainio, J. Peltola, S. Persijn, F. J. M. Harren and L. Halonen, Appl. Phys. B, 2009, 94, 411–427.
53 D.R. Hall and P.E. Jackson, *The Physics and Technology of Laser Resonators*, Taylor & Francis, New York, 1989.
54 M. M. J. W. Van Herpen, S. Li, S. E. Bisson, S. te Lintel Hekkert and F. J. M. Harren, *Appl. Phys. B*, 2002, **75**, 329-333.
55 C. R. Phillips and M. M. Fejer, *J. Opt. Soc. Am. B*, 2010, **27**, 2687-2699.
56 A. Henderson and R. Stafford, *Opt. Lett*., 2007, **32**, 1281-1283.
57 J. Kiessling, R. Sowade, I. Breunig, K. Buse and V. Dierolf, *Opt. Express*, 2008, **17**, 87-91.
58 M. Vainio, J. Peltola, S. Persijn, F. J. M. Harren and L. Halonen, *Opt. Express*, 2008, **16**, 11141-11146.
59 M. Vainio, M. Merimaa and L. Halonen, *Opt. Lett.*, 2011, **36**, 4122-4124.
60 A. K. Y. Ngai, S. T. Persijn, G. Von Basum and F. J. M. Harren, *Appl. Phys*. B, 2006, **85**, 173-180.
61 J. R. Schwesyg, C. R. Phillips, K. Ioakeimidi, M. C. C. Kajiyama, M. Falk, D. H. Jundt, K. Buse and M. M. Fejer, *Opt. Lett*., 2010, **35**, 1070-1072.
62 A. Henderson and R. Stafford, *Appl. Phys. B*., 2006, **85**, 181-184.
63 S. C. Kumar, R. Das, G. K. Samanta and M. Ebrahim-Zadeh, *Appl. Phys. B*, 2011, **102**, 31-35.
64 L. B. Kreuzer, *Proceedings of the Joint Conference on Lasers and Opto-electronics* (Institution of Electronic and Radio Engineers, 1969, 52-63.
65 R. Sowade, I. Breunig, J. Kiessling and K. Buse, *Appl. Phys. B*, 2009, **96**, 25-28.
66 P. Zeil, N. Thilmann, V. Pasiskevicius and F. Laurell, *Opt. Express*, 2014, **22**, 29907-29913.

67 S. T. Lin, Y. Y. Lin, T. D. Wang and Y. C. Huang, *Opt. Express*, 2010, **18**, 1323-1329.
68 J. R. Schwesyg, M. Falk, C. R. Phillips, D. H. Jundt, K. Buse and M. Fejer, *J. Opt. Soc. Am. B,* 2011, **28**, 1973-1987.
69 S. E. Bisson, K. M. Armstrong, T. J. Kulp and M. Hartings, *Appl. Opt*., 2001, **40**, 6049-6055.
70 M. Vainio, M. Siltanen, J. Peltola and L. Halonen, *Opt. Express*, 2009, **17**, 7702-7707.
71 M. Vainio, M. Siltanen, J. Peltola and L. Halonen, *Appl. Opt*., 2011, **50**, A1-A10.
72 M. Vainio, M. Siltanen, T. Hieta and L. Halonen, *Opt. Lett*., 2010, **35**, 1527-1529.
73 M. Vainio and L. Halonen, Opt. Lett., 2011, **36**, 475-477.
74 M. Vainio, C. Ozanam and L. Halonen, *Opt. Express*, 2011, **19**, 22515-22527.
75 K. N. Crabtree, J. N. Hodges, B. M. Siller, A. J. Perry, J. E. Kelly, P. A. Jenkins and B. J. McCall, *Chem. Phys. Lett*., 2012, **551**, 1-6.
76 O. Mhibik, T.-H. My, D. Paboeuf, F. Bretenaker and C. Drag, *Opt. Lett*., 2010, **35**, 2364-2367.
77 E. Andrieux, T. Zanon, M. Cadoret, A. Rihan and J.-J. Zondy, *Opt. Lett*., 2011, **36**, 1212-1214.
78 I. Ricciardi, S. Mosca, M. Parisi, P. Maddaloni, L. Santamaria, P. De Natale and M. De Rosa, *ArXiv*:1507.08519, 2015.
79 E. V. Kovalchuk, T. Schuldt and A. Peters, *Opt. Lett*., 2005, **30**, 3141-3143.
80 H. Inaba, T. Ikegami, F.-L. Hong, Y. Bitou, A. Onae, T. R. Schibli, K. Minoshima and H. Matsumoto, *Appl. Opt*., 2006, **45**, 4910-4915.
81 I. Ricciardi, E. De Tommasi, P. Maddaloni, S. Mosca, A. Rocco, J.-J. Zondy, M. De Rosa and P. De Natale, *Opt. Express*, 2012, **20**, 9178-9186.
82 O. Asvany, J. Krieg and S. Schlemmer, *Rev. Sci. Instrum*., 2012, **83**, 093110.
83 J. Peltola, M. Vainio, T. Fordell, T. Hieta, M. Merimaa and L. Halonen, *Opt. Express*, 2014, **22**, 32429-32439.
84 M. Siltanen, M. Vainio and L. Halonen, *Opt. Express*, 2010, **18**, 14087-14092.
85 A. M. Morrison, T. Liang and G. E. Douberly, *Rev. Sci. Instrum*., 2013, **84**, 013102.
86 J. Krieg, A. Klemann, I. Gottbehüt, S. Thorwirth, T. F. Giesen and S. Schlemmer, *Rev. Sci. Instrum*., 2011, **82**, 063105.
87 P. Gross, M. E. Klein, T. Walde, K.-J. Boller, M. Auerbach, P. Wessels and C. Fallnich, *Opt. Lett*. 2002, **27**, 418-420.
88 X. Hong, X. Shen, M. Gong and F. Wang, *Opt. Lett*., 2012, **37**, 4982-4984.
89 J. Courtois, R. Bouchendira, M. Cadoret, I. Ricciardi, S. Mosca, M. De Rosa, P. De Natale and J.-J. Zondy, *Opt. Lett.*, 2013, **38**, 1972-1974.
90 I. D. Lindsay, B. Adhimoolam, P. Groß, M. E. Klein and K. -J. Boller, *Opt. Express*, 2005, **13**, 1234-1239.
91 D. D. Arslanov, M. Spunei, A. K. Y. Ngai, S. M. Cristescu, I. D. Lindsay, S. T. Persijn, K. J. Boller, F. J. M. Harren, *Appl. Phys. B*, 2011, **103**, 223-228.
92 D. D. Arslanov, M. Spunei, J. Mandon, S. M. Cristescu, S. T. Persijn, and F. J. M. Harren, *Laser Photon. Rev*., 2013, **7**, 188-206.
93 P. E. Powers, Thomas J. Kulp and S. E. Bisson, *Opt. Lett*., 1998, **23**, 159-161.
94 I. Breunig, J. Kiessling, B. Knabe, R. Sowade and K. Buse, *Opt. Express*, 2008, **16**, 5662-5666.
95 M. Siltanen, T. Leinonen and L. Halonen, *Opt. Express*, 2011, **19**, 19675-19680.
96 C. S. Werner, K. Buse and I. Breunig, *Opt. Lett*., 2015, **40**, 772-774.
97 C. R. Phillips, J. S. Pelc and M. M. Fejer, *Opt. Lett*., 2011, **36**, 2973-2975.
98 S. Orlov, W. Grundkötter, D. Hofmann, V. Quiring, R. Ricken, H. Suche and W. Sohler, *Mid-Infrared Coherent Sources and Applications*, 377-392, Springer, 2008.
99 C. Ozanam, M. Savanier, L. Lanco, X. Lafosse, G. Almuneau, A. Andronico, I. Favero, S. Ducci and G. Leo, *J. Opt. Soc. Am. B*, 2014, **31**, 542-550.
100 S. T. Cundiff and J. Ye, *Rev. Mod. Phys*., 2003, **75**, 325 –342.
101 A. Schliesser, N. Picqué and T. W. Hänsch, *Nature Photonics*, 2012, **6**, 440-449.
102 F. Adler, K. C. Cossel, M. J. Thorpe, I. Hartl, M. E. Fermann and J. Ye, *Opt. Lett*., 2009, **34**, 1330–1332.
103 N. Leindecker, A. Marandi, R. L. Byer and K. L. Vodopyanov, *Opt. Express*, 2011, **19**, 6296-6302.
104 S. Chaitanya Kumar, A. Esteban-Martin, T. Ideguchi, M. Yan, S. Holzner, T. W. Hänsch, N. Picqué and M. Ebrahim-Zadeh, *Laser Photon. Rev*., 2014, **8**, L86-L91.
105 A. Esteban-Martin, O. Kokabee, K. Moutzouris and M. Ebrahim-Zadeh, *Opt. Lett*., 2009, **34**, 428-430.
106 K. A. Ingold, A. Marandi, C. W. Rudy, K. L. Vodopyanov and R. L. Byer, *Opt. Lett.*, 2014, **39**, 900-903.
107 Y. Kobayashi, K. Torizuka, A. Marandi, R. L. Byer, R. A. McCracken, Z. Zhang and D. T. Reid, *J. Opt*., 2015, **17**, 094010.
108 A. Marandi, N. C. Leindecker, V. Pervak, R. L. Byer and K. L. Vodopyanov, *Opt. Express*, 2012, **20**, 7255-7262.
109 K. F. Lee, J. Jiang, C. Mohr, J. Bethge, M. E. Fermann, N. Leindecker, K. L. Vodopyanov, P. G. Schunemann and I. Hartl, *Opt. Lett*., 2013, **38**, 1191-1193.
110 N. Leindecker, A. Marandi, R. L. Byer, K. L. Vodopyanov, J. Jiang, I. Hartl, M. Fermann and P. G. Schunemann, *Opt. Express*, 2012, **20**, 7046-7053.
111 K. L. Vodopyanov, E. Sorokin, I. T. Sorokina and P. G. Schunemann, *Opt. Lett*., 2011, **36**, 2275-2277.
112 V. O. Smolski, S. Vasilyev, P. G. Schunemann, S. B. Mirov and K. L. Vodopyanov, *Opt. Lett.,* 2015, **40**, 2906-2908.
113 A. Marandi, K. A. Ingold, M. Jankowski and R. L. Byer, *ArXiv*:1510.03744, 2015.
114 K. Balskus, Z. Zhang, R. A. McCracken and D. T. Reid, *Opt. Lett*., 2015, **40**, 4178-4181.
115 K. C. Burr, C. L. Tang, M. A. Arbore and M. M. Fejer, *Opt. Lett*., 1997, **22**, 1458-1460.
116 Z. Zhang, C. Gu, J. Sun, C. Wang, T. Gardiner and D. T. Reid, *Opt. Lett*., 2012, **37**, 187-189.
117 Y. Jin, S. M. Cristescu, F. J. M. Harren, and J. Mandon, *Opt. Lett*., 2014, **39**, 3270–3273.

118 Z. Zhang, T. Gardiner and D. T. Reid, *Opt. Lett*., 2013, **38**, 3148-3150.
119 Y. Jin, S. M. Cristescu, F. J. M. Harren and J. Mandon, *Appl. Phys. B*, 2015, **119**, 65–74.
120 P. Domachuk, N. A. Wolchover, M. Cronin-Golomb, A. Wang, A. K. George, C.M.B. Cordeiro, J.C. Knight and F. G. Omenetto, *Opt. Express*, 2008, **16**, 7161-7168.
121 C. W. Rudy, A. Marandi, K. L. Vodopyanov and R. L. Byer, *Opt. Lett*., 2013, **38**, 2865-2868.
122 A. Marandi, C. W. Rudy, V. G. Plotnichenko, E. M. Dianov, K. L. Vodopyanov and R. L. Byer, *Opt. Express*, 2012, 20, 24218-24225.
123 K. F. Lee, N. Granzow, M. A. Schmidt, W. Chang, L. Wang, Q. Coulombier, J. Troles, N. Leindecker, K. L. Vodopyanov, P. G. Schunemann, M. E. Fermann, P. St. J. Russell and I. Hartl, *Opt. Lett*., 2014, **39**, 2056-2059.
124 B. Kuyken, T. Ideguchi, S. Holzner, M. Yan, T. W. Hänsch, J. Van Campenhout, P. Verheyen, S. Coen, F. Leo, R. Baets, G. Roelkens, and N. Picqué, *Nat. Commun*., 2015, **6**, 6310-6315.
125 C. R. Phillips, C. Langrock, J. S. Pelc, M. M. Fejer, J. Jiang, M. E. Fermannand I. Hartl, *Opt. Lett*., 2011, **36**, 3912-3914.
126 P. Maddaloni, P. Malara, G. Gagliardi and P. De Natale, *New J. Phys*, 2006, **8**, 262-269.
127 I. Galli, F. Cappelli, P. Cancio, G. Giusfredi, D. Mazzotti, S. Bartalini and P. De Natale, *Opt. Express*, 2013, **21**, 28877-28885.
128 C. Erny, K. Moutzouris, J. Biegert, D. Kühlke, F. Adler, A. Leitenstorfer and U. Keller, *Opt. Lett*., 2007, **32**, 1138-1140.
129 F. C. Cruz, D. L. Maser, T. Johnson, G. Ycas, A. Klose, F. R. Giorgetta, I. Coddington and S. A. Diddams, *Opt. Express*, 2015, **23**, 26814-26824.
130 T. W. Neely, T. A. Johnson and S. A. Diddams, *Opt. Lett*., 2011, **36**, 4020-4022.
131 A. Ruehl, A. Gambetta, I. Hartl, M. E. Fermann, K. S. E. Eikema and M. Marangoni, *Opt. Lett*., 2012, **37**, 2232-2234.
132 D. G. Winters, P. Schlup and R. A. Bartels, *Opt. Lett*., 2010, **35**, 2179-2180.
133 C. R. Phillips, J. Jiang, C. Mohr, A. C. Lin, C. Langrock, M. Snure, D. Bliss, M. Zhu, I. Hartl, J. S. Harris, M. E. Fermann and M. M. Fejer, *Opt. Lett*., 2012, **37**, 2928-2930.
134 T. Steinle, A. Steinmann, R. Hegenbarth and H. Giessen, *Opt. Express*, 2014, **22**, 9567-9573.
135 T. Hu, S. D. Jackson and D. D. Hudson, *Opt. Lett*., 2015, **40**, 4226-4228.
136 A. Hugi, G. Villares, S. Blaser, H. C. Liu and J. Faist, *Nature*, 2012, **492**, 229-233.
137 T. J. Kippenberg, R. Holzwarth and S. A. Diddams, *Science*, 2011, **332**, 555-559.
138 A. G. Griffith, R. K. W. Lau, J. Cardenas, Y. Okawachi, A. Mohanty, R. Fain, Y. H. D. Lee, M. Yu, C. T. Phare, C. B. Poitras, A. L. Gaeta and M. Lipson, *Nat. Commun*., 2015, **6**, 6299-6303.
139 A. A. Savchenkov, V. S. Ilchenko, F. Di Teodoro, P. M. Belden, W. T. Lotshaw, A. B. Matsko and L. Maleki, *Opt. Lett*., 2015, **40**, 3468-3471.
140 C. Lecaplain, C. Javerzac-Galy, E. Lucas, J. D. Jost, T. J. and Kippenberg, *ArXiv*:1506.00626, 2015.
141 V. Ulvila, C. R. Phillips, L. Halonen and M. Vainio, Opt. Lett., 2013, 38, 4281-4284.
142 I. Ricciardi, S. Mosca, M. Parisi, P. Maddaloni, L. Santamaria, P. De Natale and M. De Rosa, *Phys. Rev. A*, 2015, **91**, 063839-1-063839-10.
143 V. Ulvila, C. R. Phillips, L. Halonen and M. Vainio, *Phys. Rev. A*, 2015, **92**, 033816.
144 S. Mosca, I. Ricciardi, M. Parisi, P. Maddaloni, L. Santamaria, P. De Natale and M. De Rosa, *arXiv: 1510.08074*, 2015.
145 V. Ulvila, C. R. Phillips, L. Halonen and M. Vainio, *Opt. Express*, 2014, **22**, 10535-10543.
146 M. R. McCurdy, Y. Bakhirkin, G. Wysocki, R. Lewicki and F. K. Tittel, *J. Breath Res*., 2007, **1**, 014001.
147 K. P. Petrov, A. T. Ryan, T. L. Patterson, L. Huang, S. J. Field, and D. J. Bamford, *Opt. Lett*., 1998, **23**, 1052-1054.
148 K. P. Petrov, L. Goldberg, W. K. Burns, R. F. Curl and F. K. Tittel, *Opt. Lett*., 1996, **21**, 86-88.
149 D. G. Lancaster, D. Richter, R. F. Curl, F. K. Tittel, L. Goldberg and J. Koplow, *Opt. Lett*., 1999, **24**, 1744-1746.
150 M. van Herpen, S. te Lintel Hekkert, S. E. Bisson and F. J. M. Harren, *Opt. Lett*., 2002, **27**, 640-642.
151 F. K. Tittel, D. Richter and A. Fried, *Solid-State Mid-Infrared Laser Sources* (*Mid-Infrared Laser Applications in Spectroscopy*), *Topics Appl. Phys*. **89**, 445-516, Springer-Verlag Berlin Heidelberg, 2003.
152 U. Gustafsson, J. Sandsten and S. Svanberg, *Appl. Phys. B*, 2000, **71**, 853-857.
153 D. Mazzotti, P. De Natale, G.Giusfredi, C. Fort, J.A. Mitchell and L.W. Hollberg, *Appl. Phys. B*, 2000, **70**, 747-750.
154 D. G. Lancaster, D. Richter, R. F. Curl, F. K. Tittel, L. Goldberg and J. Koplow, *Opt. Lett*., 1999, **24**, 1744-1746.
155 G. B. Rieker, F. R. Giorgetta, W. C. Swann, J. Kofler, A. M. Zolot, L. C. Sinclair, E. Baumann, C. Cromer, G. Petron, C. Sweeney, P. P. Tans, I. Coddington and N. R. Newbury, *Optica*, 2014, **1**, 290-298.
156 K. P. Petrov, R. F. Curl and F. K. Tittel, *Appl. Phys. B*, 1998, **66**, 531-538.
157 J. Cousin, W. Chen, D. Bigourd, M. Fourmentin and S. Kassi, *Appl. Phys. B*, 2009, **97**, 919-929.
158 M. Erdélyi, D. Richter and F. K. Tittel, *Appl. Phys. B*, 2002, **75**, 289-295.
159 H. Waechter and M. W. Sigrist, *Appl. Phys. B*, 2007, **87**, 539-546.
160 E. Kerstel and L. Gianfrani, *Appl. Phys. B*, 2008, **92**, 439-449.
161 J. A. Silver, *Appl. Opt*., 1992, **31**, 707-717.
162 P. Maddaloni, P. Malara, G. Gagliardi and P. De Natale, *Appl. Phys. B*, 2006, **85**, 219-222.
163 D. Richter, A. Fried, B. P. Wert, J. G. Walega and F. K. Tittel, *Appl. Phys. B*, 2002, **75**, 281-288.
164 I.D. Lindsay, P. Groß, C.J. Lee, B. Adhimoolam and K.-J. Boller, *Opt. Express*, 2006, **14**, 12341-12346.
165 P. Kluczynski and O. Axner, *Appl. Opt*., 1999, **38**, 5803-5815.
166 P. Kluczynski, J. Gustafsson, Å. M. Lindberg and O. Axner, *Spectrochim. Acta Part B*, 2001, **56**, 1277–1354.
167 S. Persijn, F. Harren and A. van der Veen, *Appl. Phys. B*, 2010, **100**, 383-390.

168 A. O'Keefe, J. J. Scherer and J. B. Paul, *Chem. Phys. Lett*., 1999, **307**, 343–349.
169 D. Herriott, H. Kogelnik and R. Kompfner, *Appl. Opt*., 1964, **3**, 523-526.
170 P. Maddaloni, G. Gagliardi, P. Malara and P. De Natale, *J. Opt. Soc. Am. B*, 2006, **23**, 1938-1945.
171 P. Malara, P. Maddaloni, G. Gagliardi and P. De Natale, *Opt. Express*, 2006, **14**, 1304-1313.
172 J. J. Scherer, J. B. Paul, H. J. Jost and M. L. Fischer, *Appl. Phys. B*, 2013, **110**, 271-277.
173 D. D. Arslanov, S. M. Cristescu and F. J. M. Harren, *Opt. Lett*., 2010, **35**, 3300-3302.
174 D. D. Arslanov, K. Swinkels, S. M. Cristescu and F. J. M. Harren, *Opt. Express*, 2011, **19**, 24078-24089.
175 D. Romanini, A. A. Kachanov, N. Sadeghi and F. Stoeckel, *Chem. Phys. Lett*., 1997, **264**, 316–322.
176 G. von Basum, D. Halmer, P. Hering, M. Mürtz, S. Schiller, F. Müller, A. Popp, and F. Kühnemann, *Opt. Lett*., 2004, **29**, 797-799.
177 J. Courtois, A.K. Mohamed and D. Romanini, *Opt. Express*, 2010, **18**, 4845-4858.
178 J. Peltola, M. Vainio, V. Ulvila, M. Siltanen, M. Metsälä and L. Halonen, *Appl. Phys. B*, 2012, **107**, 839-847.
179 F. J. M. Harren, G. Cotti, J. Oomens and S. te Lintel Hekkert, *Encyclopedia of Analytical Chemistry* (Photoacoustic Spectroscopy in Trace Gas Monitoring, 2203-2226), John Wiley & Sons Ltd, Chichester, 2000.
180 J. Ng, A. H. Kung, A. Miklós and P. Hess, *Opt. Lett*., 2004, **29**, 1206-1208.
181 J. Peltola, M. Vainio, T. Hieta, J. Uotila, S. Sinisalo, M. Metsälä, M. Siltanen and L. Halonen, *Opt. Express*, 2013, **21**, 10240-10250.
182 F. Kühnemann, K. Schneider, A. Hecker, A.A.E. Martis, W. Urban, S. Schiller, and J. Mlynek, *Appl. Phys. B*, 1998, **66**, 741-745.
183 M. M. J. W. van Herpen, S. Li, S. E. Bisson and F. J. M. Harren, *Appl. Phys. Lett*., 2002, **81**, 1157-1159.
184 M. M. J. W. van Herpen, A. K. Y. Ngai, S. E. Bisson, J. H. P. Hackstein, E. J. Woltering and F. J. M. Harren, *Appl. Phys. B*, 2006, **82**, 665-669.
185 D. D. Arslanov, M. P. Castro, N. A. Creemers, A. H. Neerincx, M. Spunei, J. Mandon, S. M. Cristescu, P. Merkus and F. J. Harren, *J. Biomed. Opt*., 2013, **18**, 107002.
186 L. Dong, A. A. Kosterev, D. Thomazy and F. K. Tittel, *Appl. Phys. B*, 2010, **100**, 627-635.
187 J. Kauppinen, K. Wilcken, I. Kauppinen and V. Koskinen, *Microchem. J*., 2004, **76**, 151-159.
188 A. K. Y. Ngai, S. T. Persijn, I. D. Lindsay, A. A. Kosterev, P. Groß, C. J. Lee, S. M. Cristescu, F. K. Tittel, K.-J. Boller and F. J. M. Harren, *Appl. Phys. B*, 2007, **89**, 123-128.
189 V. Spagnolo, P. Patimisco, S. Borri, G. Scamarcio, B. Bernacki and J. Kriesel, *Opt. Lett*., 2012, **37**, 4461-4463.
190 T. Laurila, H. Cattaneo, V. Koskinen, J. Kauppinen, and R. Hernberg, *Opt. Express*, 2005, **13**, 2453-2458.
191 A. Pogány, S. Wagner, O. Werhahn and V. Ebert, *Appl. Spectros*., 2015, **69**, 257-268.
192 L. S. Rothman, I. E. Gordon, Y. Babikov, A. Barbe, D. C. Benner, P. F. Bernath, M. Birk, L. Bizzocchi, V. Boudon, L. R. Brown, A. Campargue, K. Chance, E. A. Cohen, L. H. Coudert, V. M. Devi, B. J. Drouin, A. Fayt, J.-M. Flaud, R. R. Gamache, J. J. Harrison, J.-M. Hartmann, C. Hill, J. T. Hodges, D. Jacquemart, A. Jolly, J. Lamouroux, R. J. Le Roy, G. Li, D. A. Long, O. M. Lyulin, C. J. Mackie, S. T. Massie, S. Mikhailenko, H. S. P. Müller, O. V. Naumenko, A. V. Nikitin, J. Orphal, V. Perevalov, A. Perrin, E. R. Polovtseva, C. Richard, M. A. H. Smith, E. Starikova, K. Sung, S. Tashkun, J. Tennyson, G. C. Toon, V. G. Tyuterev and G. Wagner, *J. Quant. Spectrosc. Radiat. Transfer*, 2013, **130**, 4-50.
193 N. Jacquinet-Hussonn, N. Scott, A. Chedina, L. Crepeau, R. Armante, V. Capelle, J. Orphal, A. Coustenis, C. Boonne, N. Poulet-Crovisier, A. Barbee, M. Birk, L. Brown, C. Camy-Peyret, C. Claveau, K. Chance, N. Christidis, C. Clerbaux, P. Coheur, V. Dana, L. Daumont, M. D. Backer-Barilly, G. D. Lonardo, J. Flaud, A. Goldman, A. Hamdouni, M. Hess, M. Hurley, D. Jacquemart, I. Kleiner, P. Kopke, J. Mandin, S. Massie, S. Mikhailenko, V. Nemtchinov, A. Nikitin, D. Newnham, A. Perrin, V. Perevalov, S. Pinnock, L. Regalia-Jarlot, C. Rinsland, A. Rublev, F. Schreier, L. Schult, K. Smith, S. Tashkun, J. Teffo, R. Toth, V. Tyuterev, J. Auwera, P. Varanasi and G. Wagner, *J. Quant. Spectrosc. Radiat. Transf*., 2008, **109**, 1043–1059.
194 K. Knabe, P. A. Williams, F. R. Giorgetta, C. M. Armacost, S. Crivello, M. B. Radunsky and N. R. Newbury, *Opt. Express*, 2012, **20**, 12432–12442.
195 K. Knabe, P. A. Williams, F. R. Giorgetta, M. B. Radunsky, C. M. Armacost, S. Crivello and N. R. Newbury, *Opt. Express*, 2013, **21**, 1020-1029.
196 I. Galli, S. Bartalini, P. Cancio, G. Giusfredi, D. Mazzotti and P. De Natale, *Opt. Express*, 2009, **17**, 9582-9587.
197 L. Nugent-Glandorf, F. R. Giorgetta and S. A. Diddams, *Appl. Phys. B*, 2015, **119**, 327–338.
198 L. Nugent-Glandorf, T. Neely, F. Adler, A. Fleisher, K. Cossel, B. Bjork, T. Dinneen, J. Ye and S. Diddams, *Opt. Lett*., 2012, **37**, 3285-3287.
199 T. A. Johnson and S. A. Diddams, *Appl. Phys. B*, 2012, **107**, 31-39.
200 F. Adler, P. Masłowski, A. Foltynowicz, K. C. Cossel, T. C. Briles, I. Hartl and J. Ye, *Opt. Express*, 2010, **18**, 21861-21872.
201 E. Baumann, F. R. Giorgetta, W. C. Swann, A. M. Zolot, I. Coddington and N. R. Newbury, *Phys. Rev. A*, 2011, **84**, 062513.
202 N. R. Newbury, I. Coddington and W. Swann, *Opt. Express*, 2010, **18**, 7929-7945.
203 A. Foltynowicz, P. Masłowski, A.J. Fleisher, B.J. Bjork and J. Ye, *Appl. Phys. B*, 2013, **110**, 163-175.
204 F. Adler, M. J. Thorpe, K. C. Cossel and J. Ye, *Annu. Rev. Anal. Chem*., 2010, **3**, 175–205.
205 P. Masłowski, K.C. Cossel, A. Foltynowicz and J. Ye, *Cavity-Enhanced Spectroscopy and Sensing*, Ch. 8, Springer-Verlag Berlin Heidelberg, 2014.
206 M. W. Haakestad, T. P. Lamour, N. Leindecker, A. Marandi and K. L. Vodopyanov, *J. Opt. Soc. Am. B*, 2013, **30**, 631-640.

207 P. Maslowski, K. F. Lee, A. C. Johansson, A. Khodabakhsh, G. Kowzan, L. Rutkowski, A. A. Mills, C. Mohr, J. Jiang, M. E. Fermann and A. Foltynowicz, *arXiv:1505.07706*, 2015.
208 S. Schiller, *Opt. Lett*., 2002, **27**, 766-768.
209 F. Keilmann, C. Cohle and R. Holzwarth, *Opt. Lett*., 2004, **29**, 1542-1544.
210 D. A. Long, A. J. Fleisher, K. O. Douglass, S. E. Maxwell, K. Bielska, J. T. Hodges and F. Plusquellic, *Opt. Lett*., 2014, **39**, 2688-2690.
211 I. Znakovskaya, E. Fill, N. Forget, P. Tournois, M. Seidel, O. Pronin, F. Krausz and A. Apolonski, *Opt. Lett*., 2014, **39**, 5471–5474.
212 P. Martín-Mateos, B. Jerez and P. Acedo, *Opt. Express*, 2015, **23**, 21149-21158.
213 S. M. Link, A. Klenner, M. Mangold, C. A. Zaugg, M. Golling, B. W. Tilma and U. Keller, O*pt. Express*, 2015, **23**, 5521–5531.
214 T. Ideguchi, A. Poisson, G. Guelachvili, N. Picqué and T. W. Hänsch, *Nature Commun*., 2014, **5**, 3375.
215 D. Mazzotti, P. Cancio, G. Giusfredi, P. D. Natale, and M. Prevedelli, *Opt. Lett*., 2005, **30**, 997–999.
216 K. Takahata, T. Kobayashi, H. Sasada, Y. Nakajima, H. Inaba and F.-L. Hong, *Phys. Rev. A*, 2009, **80**, 032518.
217 A. Gambetta, D. Gatti, A. Castrillo, G. Galzerano, P. Laporta, L. Gianfrani and M. Marangoni, *Appl. Phys. Lett*., 2011, **99**, 251107.
218 S. Borri, I. Galli, F. Cappelli, A. Bismuto, S. Bartalini, P. Cancio, G. Giusfredi, D. Mazzotti, J. Faist and P. De Natale, *Opt. Lett*., 2012, **37**, 1011-1013.
219 I. Galli, M. Siciliani de Cumis, F. Cappelli, S. Bartalini, D. Mazzotti, S. Borri, A. Montori, N. Akikusa, M. Yamanishi, G. Giusfredi, P. Cancio and P. De Natale, *Opt. Express*, 2013, **102**, 121117.
220 E. Benkler, F. Rohde and H. R. Telle, *Opt. Express*, **21**, 5793 (2013).
221 F. Rohde, E. Benkler, T. Puppe, R. Unterreitmayer, A. Zach and H. R. Telle, *Opt. Lett.*, **39**, 4080 (2014).
222 M. Abe, K. Iwakuni, S. Okubo and H. Sasada, *J. Opt. Soc. Am. B*, 2013, **30**, 1027-1035.
223 S. Okubo, H. Nakayama, K. Iwakuni, H. Inaba and H. Sasada, *Opt. Express*, 2011, **19**, 23878–23888.
224 M. P. Moreno, M. Cadoret, M. Jahjah, L. Nguyen, F. C. Cruz and J.-J. Zondy, *Appl. Phys. B*, 2014, **117**, 681-687.
225 K. Iwakuni, H. Sera, M. Abe and H. Sasada, *J. Mol. Spectrosc*., 2014, **306**, 19-25.
226 I. Galli, S. Bartalini, S. Borri, P. Cancio, D. Mazzotti, P. De Natale and G. Giusfredi, *Phys. Rev. Lett*., 2011, **107**, 270802.
227 P. Cancio Pastor, I. Galli, G. Giusfredi, D. Mazzotti and P. De Natale, *Phys. Rev. A*, 2015, **92**, 063820.
228 S. Thorwirth, J. Krieg, V. Lutter, I. Keppeler, S. Schlemmer, M.E. Harding, J. Vázquez and T.F. Giesen, *J. Mol. Spectrosc*., 2011, **270**, 75–78.
229 M. Siltanen, M. Metsälä, M. Vainio and L. Halonen, *J. Chem. Phys*., 2013, **139**, 054201.
230 J. Karhu, J. Nauta, M. Vainio, M. Metsälä and L. Halonen, *Proceedings of the 24th Colloquium on High Resolution Molecular Spectroscopy*, Dijon, France, Aug 24 -28, 2015.
231 A.K.Y. Ngai, H. Verbraak, S.T. Persijn, H. Linnartz and F.J.M. Harren, *Appl. Phys. Lett*., 2007, **90**, 081109.
232 D. H. Levy, *Science*, 1981, **214**, 263-269.
233 C.-H. Chang and D. J. Nesbitt, *J. Phys. Chem. A*, 2015, **119**, 7940−7950.
234 D. Zhao, K. D. Doney and H. Linnartz, *J. Mol. Spectrosc*., 2014, **296**, 1–8.
235 H. Chadwick, P. M. Hundt, M. E. van Reijzen, B. L. Yoder and R. D. Beck, *J. Chem. Phys*., 2014, **140**, 034321.
236 D. Zhao, J. Guss, A. J. Walsh and H. Linnartz, *Chem. Phys. Lett.*, 2013, **565**, 132-137.
237 K.D. Doney, D. Zhao and H. Linnartz, *J. Mol. Spectrosc*., 2015, **316**, 54-63.
238 D. Zhao and H. Linnartz, *Chem. Phys. Lett.*, 2014, **595-596**, 256-259.
239 J. Ye, L.-S. Ma and J. L. Hall, *J. Opt. Soc. Am. B*, 1998, **15**, 6-15.
240 T. G. Spence, C. C. Harb, B. A. Paldus, R. N. Zare, B. Willke and R. L. Byer, *Rev. Sci. Instrum*., 2000, **71**, 347-353.
241 R. Z. Martínez, M. Metsälä, O. Vaittinen, T. Lantta and L. Halonen, *J. Opt. Soc. Am. B*, 2006, **23**, 727-740.
242 D. Halmer, G. von Basum, P. Hering and M. Mürtz, *Opt. Lett*., 2005, **30**, 2314-2316.
243 D. A. Long, G.-W. Truong, R. D. van Zee, D. F. Plusquellic and J. T. Hodges, *Appl. Phys. B*, 2014, **114**, 489-495.
244 A. Foltynowicz, F.M. Schmidt, W. Ma and O. Axner, *Appl. Phys. B*., 2008, **92**, 313-326.
245 R. W. P. Drever, J. L. Hall, F. V. Kowalski, J. Hough, G. M. Ford, A. J. Munley and H. Ward, *Appl. Phys. B*, 1983, **31**, 97-105.
246 E. D. Black, *Am. J. Phys*., 2001, **69**, 79.
247 M. S. Taubman, T. L. Myers, B. D. Cannon and R. M. Williams, *Spectrochim. Acta Part A*, 2004, **60**, 3457-3468.
248 M. W. Porambo, B. M. Siller, J. M. Pearson and B. J. McCall, *Opt. Lett*., 2012, **37**, 4422.
249 I. Silander, T. Hausmaninger, W. Ma, F. J. M. Harren and O. Axner, *Opt. Lett*., 2015, **40**, 439-442.
250 H. Verbraak, A.K.Y. Ngai, S.T. Persijn, F.J.M. Harren and H. Linnartz, *Chem. Phys. Lett*., 2007, **442**, 145-149.
251 B. M. Siller, J. N. Hodges, A. J. Perry and B. J. McCall, *J. Phys. Chem. A*., 2013, **117**, 10034−10040.
252 B. M. Siller, M. W. Porambo, A. A. Mills and B. J. McCall, *Opt. Express*, 2011, **19**, 24822.
253 K. N. Crabtree, J. N. Hodges, B. M. Siller, A. J. Perry, J. E. Kelly, P. A. Jenkins II and B. J. McCall, *Chem. Phys. Lett*., 2012, **551**, 1-6.
254 J. N. Hodges, A. J. Perry, P. A. Jenkins II, B. M. Siller and B. J. McCall, *J. Chem. Phys*., 2013, **129**, 164201.
255 C. S. Gudeman, M. H. Begemann, J. Pfaff and R. J. Saykally, *Phys. Rev. Lett*., 1983, **50**, 727-731.
256 L. C. Sinclair, K. C. Cossel, T. Coffey, J. Ye and E. A. Cornell, *Phys. Rev. Lett*., 2011, **107**, 093002.
257 S. Gärtner, J. Krieg, A. Klemann, O. Asvany, S. Brünken and S. Schlemmer, *J. Phys. Chem*., 2013, **117**, 9975-9984.
258 S. Brünken, L. Kluge, A. Stoffels, O. Asvany and S. Schlemmer, *Astrophys. J*., 2014, **783**, L4.
259 O. Asvany, K. M. T. Yamada, S. Brünken, A. Potapov and S. Schlemmer, *Science*, 2015, **347**, 1346–1349.
260 P. Jusko, O. Asvany, A.-C. Wallerstein, S. Brünken and S. Schlemmer, *Phys. Rev. Lett.*, 2014, **112**, 253005.

261 M. Y. Choi, G. E. Douberly, T. M. Falconer, W. K. Lewis, C. M. Lindsay, J. M. Merritt, P. L. Stiles and R. E. Miller, *Int. Rev. Phys. Chem.*, 2006, **25**, 15-75.
262 K. Marushkevich, M. Siltanen, M. Räsänen, L. Halonen and L. Khriachtchev, *J. Phys. Chem. Lett*., 2011, **2**, 695-699.
263 T. Liang, D. B. Magers, P. L. Raston, W. D. Allen and G. E. Douberly, J. *Phys. Chem. Lett*., 2013, **4**, 3584-3589.
264 S. D. Flynn, D. Skvortsov, A. M. Morrison, T. Liang, M. Y. Choi, G. E. Douberly and A. F. Vilesov, *J. Phys. Chem. Lett*., 2010, **1**, 2233-2238.
265 G. E. Douberly, P. L. Raston, T. Liang, M. D.Marshall, *J. Chem. Phys*. 2015, **142**, 134306
266 L.F. Gomez, R. Sliter, D. Skvortsov, H. Hoshina, G.E. Douberly and A.F. Vilesov, J. Phys. Chem. A, 2013, 117, 13648-13653.
267 F. J. Hernandez, J. T. Brice, C. M. Leavitt, G. A. Pino and G. E. Douberly, *J. Phys. Chem. A*, 2015, **119**, 8125-8132.
268 A. M. Morrison, S. D. Flynn, T. Liang and G. E. Douberly, *J. Phys. Chem. A*., 2010, **114**, 8090-8098.
269 D. Habig, D. Leicht, M. Kaufmann, G. Schwaab and M. Havenith, *J. Chem. Phys*., 2014, **141**, 044312.
270 D. Habig, D. Leicht, G. Schwaab and M. Havenith, *J. Chem. Phys*., 2015, **143**, 024308.
271 D. Leicht, D. Habig, G. Schwaab and M. Havenith, *J. Phys. Chem. A*, 2015, **119**, 1007-1012.
272 K.-K. Ni, S. Ospelkaus, M. H. G. de Miranda, A. Pe'er, B. Neyenhuis, J. J. Zirbel, S. Kotochigova, P. S. Julienne, D. S. Jin and J. Ye, *Science*, 2008, **322**, 231-235.
273 S. Ospelkaus, K.-K. Ni, D. Wang, M. H. G. de Miranda, B. Neyenhuis, G. Quéméner, P. S. Julienne, J. L. Bohn, D. S. Jin and J. Ye, *Science*, 2010, **327**, 853-857.
274 A. A. Madej, J. D. Sankey, G. R. Hanes, K. J. Siemsen and A. R. W. McKellar, *Phys. Rev. A*, 1992, **45**, 1742.
275 Y. N. Martinez de Escobar, P.G. Mickelson, M. Yan, B. J. DeSalvo, S. B. Nagel and T. C. Killian, *Phys. Rev. Lett*., 2009, **103**, 200402.
276 A. Traverso, R. Chakraborty, Y. N. Martinez de Escobar, P. G. Mickelson, S. B. Nagel, M. Yan and T. C. Killian, *Phys. Rev. A*, 2009, **79**, 060702(R).
277 Y. N. Martinez de Escobar, P. G. Mickelson, P. Pellegrini, S. B. Nagel, A. Traverso, M. Yan, R. Côté and T. C. Killian, *Phys. Rev. A*, 2008, **78**, 062708.
278 L. D. Carr, D. DeMille, R. V. Krems and J. Ye, *New J. Phys*., 2009, **11**, 055049.
279 S. Kuma and T. Momose, *New J. Phys*., 2009, **11**, 055023.
280 H. Chadwick and R. D. Beck, *Chem. Soc. Rev*., 2015, Advance Article.
281 P. M. Hundt, B. Jiang, M. E. van Reijzen, H. Guo and R. D. Beck, *Science*, 2014, **344**, 504-507.
282 B. L. Yoder, R. Bisson and R. D. Beck, *Science*, 2010, **329**, 553-556.
283 P. M. Hundt, R. Bisson and R. D. Beck, *J. Chem. Phys*., 2012, **137**, 074701.
284 P. M. Hundt, M. E. van Reijzen, H. Ueta and R. D. Beck, *J. Phys. Chem. Lett*., 2014, **5**, 1963–1967.
285 A. J. Fleisher, B. J. Bjork, T. Q. Bui, K. C. Cossel, M. Okumura and J. Ye, *J. Phys. Chem. Lett*., 2014, **5**, 2241–2246.
286 B. Sheehy, J. D. D. Martin, L. F. DiMauro, P. Agostini, K. J. Schafer, M. B. Gaarde and K. C. Kulander, *Phys. Rev. Lett*., 1999, **83**, 5270–5273.

